NORTHWESTERN UNIVERSITY

Spatial Polarity of Human Genes within Nuclei and Its Relationship to Cellular Organization

A DISSERTATION

SUBMITTED TO THE GRADUATE SCHOOL
IN PARTIAL FULFILLMENTS OF THE REQUIREMENTS

for the degree

DOCTOR OF PHILOSOPHY

Field of Driskill Graduate Training Program in Life Sciences

By

Arturo Garza-Gongora

EVANSTON, ILLINOIS

December 2018

Abstract

The blueprint of life is contained within the sequence of an organism's genome. While virtually all cells of an individual multicellular eukaryotic organism contain a near identical code of nucleic acid sequences, an organism must give rise to and maintain a varied set of cells and phenotypes. As such, sequence alone does not explain the functional outcome of building life. The cells of an organism carry out a diverse set of functions by spatiotemporally regulating gene expression. It has long been understood that histone modifications and chromatin compaction can affect the permissibility of transcription of any one gene. Nuclear organization and the compartmentalization of DNA within the nucleus are emerging as important regulators in establishing patterns of gene expression. In particular, the radial distribution of genes and chromosomes has been shown to have a defined pattern, with active transcription and gene rich chromosomes occupying the nuclear interior, and gene poor chromosomes and silenced, developmentally regulated gene loci positioned at the nuclear periphery. Furthermore, DNA can spatially associate with nuclear activity "hotspots", such as those that occur in nuclear bodies, to facilitate nuclear processes. However, the nucleus is inextricably tied to the cell in which it resides, and a long-standing question that remains to be determined is whether the subnuclear localization of gene loci is related to the extra-nuclear activity in the rest of the cell. Here, using a model of epidermal differentiation as a model of cell polarity, we test the hypothesis that the spatial localization of genes is related to the cellular localization of their encoded proteins. We find that genes that encode components of hemidesmosomes (HDs) are spatially polarized in the nucleus towards the sites of their proteins in organotypic raft cultures that recapitulate epidermal differentiation and in migrating keratinocytes. We also demonstrate that gene polarity within the nucleus impacts the asymmetric distribution of HD mRNAs in the cytoplasm. Furthermore, we

find that disruption of the interaction with the extracellular substrate and perturbation of the linker of nucleoskeleton and cytoskeleton (LINC) complex results in the coincident loss of polarized HD gene positioning and distribution of their encoded protein and mRNA. Our results indicate that spatial genome organization and cellular organization are inherently intertwined, and that nuclear gene polarity plays an important role in establishing tissue asymmetry and cell identity.

Acknowledgements

I've come to realize that science is an arduous process that inevitably comes with many failures and frustrations. While my time in graduate school definitely had its moments of defeat and despair, I've been lucky enough to be surrounded by many wonderful people to keep me cheerful and motivated.

Above all, I would like to thank my parents, Arturo Garza-Gongora, Sr. and Silvia Garza-Gongora, for never doubting. Your endless love and support has provided me with the courage to pursue my passion, and for that, I am grateful. All my successes in life, I can directly attribute to you. Thank you.

I would like to thank my thesis committee members for your invaluable suggestions, contributions, and constructive criticisms that have helped me shape the avenues of my research project and career trajectory. Brian Mitchell, thank you for always keeping an open door. Your genuine interest and unsolicited advice on my career progression is something that I truly appreciate. You may not have realized it, but you were a second mentor to me. Milan Mrksich, thank you for opening up your lab to me and for being so generous with scientific equipment, resources and experimental assistance. While our collaborative project had its share of setbacks, I'm confident it holds great promise for future investigation. Robert Goldman, thank you for providing a refreshing outlook on my project. I experienced my fair share of tunnel vision, but with your experience in the field of nuclear organization, you kept my eyes open. Also thank

you for caring about the well being of graduate students in our department. It made my time in the lab a bit less stressful.

I would also like to thank Ashley Wood, for providing direction when I most desperately needed it the most. I am still a little lost sometimes, but I'm not completely wandering aimlessly in life, as I would have been without your guidance. I never asked for your continued support, but you selflessly provided it, and of all people that have contributed to my learning, I owe my development as a scientist in the lab to you the most.

Brian Poll, thanks for taking the initial lead on the nuclear polarity experiments and providing me the foundation for which to base my thesis on. I know the pilot experiments were incredibly frustrating, but you were resilient and it paid off.

I would like to thank Bridget Henley, for simply being present. The joy that I get from the time I spend with you outside of the lab influences my state of well-being in the lab. You have enriched my life and have made me a much happier person. I look forward to keep spending time with you whenever and wherever that may be.

I would like to thank the rest of my lab mates, past and present: Danielle Fanslow, Agnes Laskowski, Erica Smith, Kyle Laster, Chelsee Strojny, Dan Neems, Lexi Cogswell, Ellen Rice, and Michael Gutbrod. You all made the lab a wonderful place to spend my time everyday. It's such a rarity that everyone I have worked with in the lab is such a positive and fantastic person. I don't think it's a coincidence that we ended up together.

To my mentor Steven Kosak, I would like to deeply express my gratitude for providing me the opportunity to work alongside you in your lab. You have challenged me intellectually, sometimes brutally so, to push forward with the most novel of ideas in a field that we both probably feel is moving in different directions. You have never been afraid to ask the difficult questions, and your relentless pursuit of the most interesting problems in nuclear organization has kept me inspired throughout grad school. Your *big picture* way of thinking has rubbed off on me, and it has made me a better scientist. The time I spent in your lab was incredibly fulfilling, and I do not regret any of it. Thank you for it all.

Finally, to my family and friends too numerous to mention, thank you for your companionship and for keeping me sane. I would not have made it alone.

Dedication

To my parents.

Table of Contents

List of Figures and Tables

Figures:

Tables:

CHAPTER I

Introduction

The nucleus is a functionally compartmentalized organelle that contains an organism's genetic material. Each normal diploid cell of the human body contains two copies of 23 distinct chromosomes, which, if laid out end-to-end, measure approximately two meters in length. Therefore, these cells are presented with an interesting problem: how to package two meters of DNA into a nucleus that is only a few micrometers in diameter. The genetic material does not exist as naked DNA within the nucleus, but rather it is associated with nucleosomes to condense and package the genome within the confines of nuclear space. DNA within the nucleus is wrapped around these repeating units of core nucleosome histone octamers, which compact DNA and further form higher order structures. Covalent modifications to histones can affect the accessibility of the DNA it is bound to and recruit regulatory proteins to regulate gene expression. However, given that the nuclear environment is exceptionally crowded and regulatory proteins tend to be confined to certain nuclear regions, histone modifications alone do not explain the entirety of gene regulation. Thus, the nucleus forms functional centers and characteristic organizational patterns to regulate gene expression. In this body of work, we examine these nuclear organizational patterns and their functional consequences. Furthermore, we use epidermal differentiation as a model to experimentally test the relationship between the spatial organization of genes within nuclei and the sites of activity of their encoded proteins within the cell. Finally, we discuss the potential mechanisms for these interactions, how these organizational patterns are established, and their impact on gene expression at the single cell level.

Genome organization

The eukaryotic genome is organized into chromatin, which allows DNA to be packaged and regulated within nuclei during interphase. Beyond the diametric properties of euchromatin and heterochromatin, gene loci and chromosomes are spatially and functionally localized in the nucleus. The organization of the eukaryotic genome into chromosome territories (CTs) plays a large role in dictating the three dimensional spatial organization of the nucleus. The fact that DNA in eukaryotic interphase nuclei consists of individual chromosomes that occupy discrete, territorial spaces in the nucleus was fist experimentally confirmed in seminal experiments using laser irradiation of interphase nuclei (1). It was observed that, in metaphase spreads of interphase laser-irradiated nuclei, the site of irradiation was restricted to large, discrete regions on few chromosomes, indicating that chromosomes within interphase nuclei occupy distinct positions, as opposed to intermixing in a "spaghetti-in-a-bowl"-like fashion (2). As CTs have become more increasingly studied, it has become apparent that the location of individual CTs within interphase nuclei is non-random. In some cases, larger chromosomes tend to be positioned peripherally and smaller chromosomes tend to be found internally within the nucleus (3). Furthermore, chromosomes may also be positioned relative to gene density, as gene poor chromosomes are found more peripherally and gene dense chromosomes are found more centrally in nuclei (4). For example, HSA 18 and HSA 19 are roughly of similar size, but HSA 18 is relatively gene-poor while HSA 19 is gene rich. These chromosomes show typical positioning patterns expected of chromosomes with respect to gene density, as HSA 18 is preferentially positioned at the periphery and HSA 19 at the nuclear interior (5). The position of these chromosome orthologs is maintained in several primate species, indicating that CT positioning is an evolutionarily

conserved nuclear phenotype (6). Furthermore, beyond these aforementioned general rules of CT localization, certain CT positioning patterns have been shown to be tissue and cell type specific (7). Beyond patterns of spatial genome organization that are based on physical characteristics of chromosomes, CTs can adopt positions based on gene co-regulation. During hematopoiesis, for instance, different lineages can adopt CT proximity patterns based on similarities between gene co-regulation during differentiation (8).

It should be noted that there are exceptions to the general rule of chromatin organization in the nucleus. For example, in rod photoreceptor cells of nocturnal mammals, heterochromatin resides in the interior of nuclei, while euchromatin and actively transcribed genes are located at the nuclear periphery (9). This phenomenon is thought to have been evolved to provide a lower refractive index to permit light transmission to photoreceptors. Another example of noncanonical chromatin organization involves mouse olfactory sensory neurons, in which one olfactory allele out of thousands is chosen to be expressed, while the others converge in interior heterochromatic foci (10). In both cases, the downregulation of lamin B receptor (LBR) as well as lamin A/C in the case of rod photoreceptors, were shown to be necessary in maintaining this "inverted" phenotype, as ectopic expression reversed the conventional organization of heterochromatin at the periphery (10, 11). This indicates that nuclear organization in metazoans is actively maintained through the presence of architectural proteins.

In addition to nuclear organization patterns observed through the positioning of whole chromosomes, individual genes can also exhibit cell-type specific patterns independent of their CTs. Looping, where DNA physically associates with regulatory elements that are not

immediately adjacent in the linear sequence, normally facilitates these processes. This phenomenon has been most well-characterized with loci that reside on the same chromosome *in cis*, such as the interaction of the locus control region with genes of the beta globin locus (12). However, gene regulation by looping *in trans* also occurs. For example, the enhancer *H* can associate with odorant receptor (OR) genes on various different chromosomes and stochastically activate one allele during olfactory receptor choice in neurons (13). It has been proposed that between CTs lies an interchromosomal space that serves as a compartment for nuclear activity to occur (14). These sites are proposed to contain a high concentration of regulatory proteins for gene regulation (15). Some genes can loop away from their CT to associate with regulatory proteins in the interchromosomal space, as has been shown with the major histocompatibility (MHC) locus among others (16). The boundaries of CTs have been shown to be sites of chromosome intermingling, providing the possibility that proximity between chromosomes can influence gene co-regulation at shared sites (17). However, localization of a gene at the periphery or away from its CT is not a prerequisite for transcriptional activation. RNA FISH experiments have shown that active genes can also localize within their CTs (18). However, though large molecules such as RNA polymerase II have been found to also localize inside CTs (19), some genes, such as the *uPa* gene, are more probe to transcriptional silencing when located inside its CT (20).

The advent of variants of the chromosome confirmation capture technique (3C), such as Hi-C, have yielded novel and unique insights into chromatin biology, such as the discovery of topologically associating domains (TADs), which are regions of the genome that tend to self-associate (21). TADs are relatively invariant across cell types and, as interactions between TADs

yield to a chromosome's emerging structure, TADs are considered the basic unit or "building blocks" of genome architecture. However, chromosome folding alone does not dictate the global organization of the genome, as the nucleus is continuously "re-wired" based on dynamic factors that yield different chromosomal topologies (22). Thus, global nuclear organization is likely formed by the concerted effects of all interacting components, which emerges as a function of self-organization.

Nuclear organization and compartmentalization of nuclear function

The idea of self-organization has been implemented as a means to conceive the dynamic organization of the genome. Self-organization in the context of nuclear cell biology has been understood as a non-hierarchical association of factors that result in functionally competent stable-state structures (23). For example, double stranded DNA repair foci have been generated in the absence of DNA breaks simply by tethering individual components of the pathway to a lac operator (lacO) array integrated into the genome (24). Similarly, nuclear bodies have been shown to self-organize using the same strategy. Immobilization of any protein component of a Cajal body to a lacO array within the nucleus is sufficient to create a Cajal body *de novo* (25).

There is an inherent promiscuity of nuclear proteins with many being involved in a wide range of networks and functions. The dynamic organization of nuclear function closely resembles a multi-

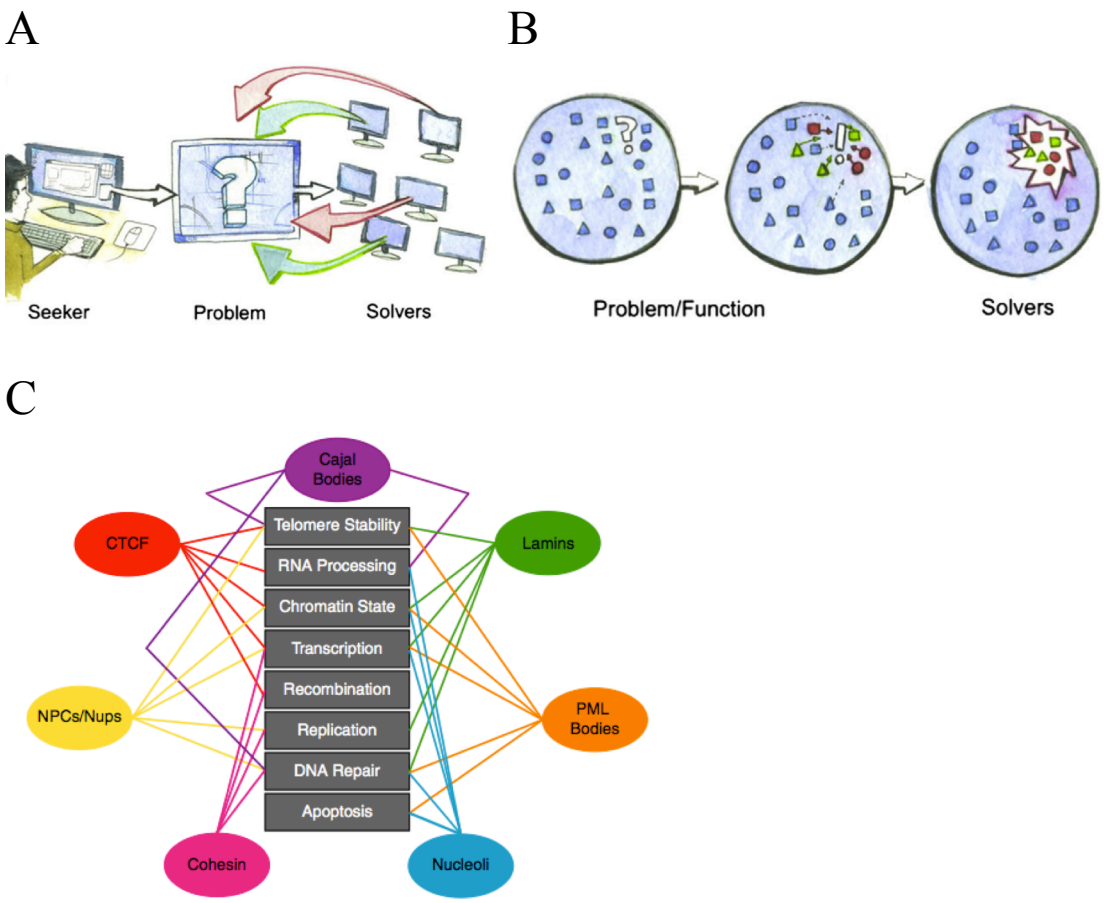

Figure 1: Nuclear crowdsourcing and the multi-functionality of nuclear bodies

A, In traditional Crowdsourcing, company or agency (the seeker), advertises a given problem to the W3. The immense 'crowd' of individuals on the W3 then participate in creating a solution to the problem based upon their avail- ability (they are aware of the challenge) and ability (they are capable of contributing to its solution). For example, red arrows represent solvers who are aware but unable to help, whereas green arrows indicate solvers who are both available and able. **B,** Crowdsourcing of nuclear function would be similar, with the notable exception of the seeker and the problem being inextricable, as the problem is the seeking entity. In parallel with (**A**) the

(Figure 1 cont.)

solvers of the function/'problem' would also have varying availability and ability. In this case availability would be whether a given agent (protein) is proximal (or dynamic enough) to engage the problem, and ability would be its capacity to function in the given process or pathway. Circles, squares, and triangles represent different classes of protein agents, with red and green shapes indicating proteins either available and/or able to participate. **C,** Nuclear proteins are connected to the pathways and functions in which they are involved, depicting not only multiplicity of function, but also the vast amount of functional overlap between the various proteins involved in nuclear organization. Figure adapted from Wood et al. (26).

agent system, with the factors involved in a particular function originating from diverse and often unexpected sources (26). We have likened this promiscuity of nuclear proteins to resemble Crowdsourcing, in which "problems", or rather nuclear functions, are carried out by a "crowd" of proteins based on their proximity, availability, and range of ability (26) (Figure 1 A-C).

The nucleus is functionally compartmentalized. In this sense, processes tend to be confined to certain regions of the nucleus, thereby facilitating coordination and execution. Transcription, for instance, can take place in certain discrete hotspots, known as "transcription factories", whereby sites enriched in active RNA polymerase II (RNAPII) provide an environment for robust gene expression. As transcription factories remain in the absence of global transcription, they represent stationary compartments as inherent sites for consolidated nuclear activity (27). Contrary to regions of the nucleus that are high in transcriptional activity, certain nuclear regions can also be inhibitive to gene expression. The nuclear periphery, which is associated with the nuclear lamin meshwork, is a largely transcriptionally repressive environment (28). To illustrate the capacity of the microenvironment at the nuclear periphery in regulating gene expression, artificially tethering a gene to the nuclear lamina is sufficient to induce it transcriptional silencing (29).

Perhaps the best example of compartmentalized nuclear activities is found in non-membranous structures known as nuclear bodies (NBs). Considered broadly, NBs are thought to manifest a potential for consolidated activity: the constituent proteins, DNA, and RNA occupy a discrete location to facilitate a collective function (30). Although NBs appear to be stable structures, their components are in fact highly dynamic, freely exchanging with a nucleoplasmic pool of protein.

Nuclear bodies often associate with chromatin, and the extent of nuclear body movement is determined by the accessibility and dynamics of the surrounding chromatin (31). Some NBs are found in a wide variety of cell types, while others are present in only a limited number of cell types and/or are formed only under certain conditions (32). In general, assigning a specific function to a particular NB has been difficult due to the large variety of constituent proteins and their involvement in many different pathways, as well as the fact that many NBs share protein interacting partners.

The promyelocytic leukemia (PML) nuclear body is a NB that exemplifies the characteristics of spatially consolidated nuclear activity. PML bodies are functionally promiscuous and dynamic structures that have been implicated in such processes as proliferation, senescence, apoptosis, genomic stability, telomere maintenance, and the DNA damage response (Figure 1C) (33). PML bodies were first observed by electron microscopy in the 1960s, and later as nuclear dots by immunofluorescence (34, 35). These nuclear dots became referred to as PML oncogenic domains (PODs), or simply PML bodies, after the discovery of the localization of the promyelocytic leukemia protein (PML), so named as it was first characterized through its fusion with the retinoic acid receptor alpha (RARA) in acute promyelocytic leukemia (APL) patients. To demonstrate the promiscuity of these nuclear bodies, over 100 proteins have been shown to localize to PML bodies, most of them transiently, or rather, under certain conditions (36). While it was initially unclear whether they simply functioned as a depository of proteins, recent work strongly indicates the role of PML bodies as functional structures whose activity is dictated by the combination of factors present at a given time. For instance, as depicted in out nuclear Crowdsourcing model, some interacting proteins can be involved in varied functions depending

on condition. This is illustrated by the interaction of PML bodies with death-associated protein 6 (DAXX), an interaction known to be involved in apoptosis and cell survival, two separate and contradictory functions (37, 38).

In addition to the functions described here, as well as other reviews elsewhere, we have identified a novel role for PML bodies in serving as sites of nuclear regulatory polypeptide synthesis. Several reports have indicated that protein synthesis occurs in the nucleus (39, 40), but both where and why it happens remains unknown. Upon the expression of aberrant RNA (*ATXN1* with a polyQ repeat expansion), the resulting protein product localizes to PML bodies (Figure 2). Furthermore, performing structured illumination microscopy combined with the ribopuromycylation method to detect nascent polypeptides, we show that nascent translation occurs at the periphery of the PML body where the PML protein is localized, and the resulting protein localizes to the interior of the nuclear body (Figure 2). We propose that this translation may represent a pioneer round of translation to detect aberrant transcripts to prevent RNA toxicity, such as that which occurs through no-go decay (41). As subnuclear bodies become further studies, it will be interesting to uncover and realize the full extent of their varied functions.

Importantly, the genomic elements can associate with subnuclear bodies for the regulation of certain nuclear processes. For example, the association of PML bodies with the *MHC* locus is well documented (42). Furthermore, the associations of PML bodies to certain genomic loci appear to be cell type dependent, highlighting the heterogeneity of PML bodies (43). Other nuclear bodies, such as Cajal bodies have been linked to genome organization (44). The

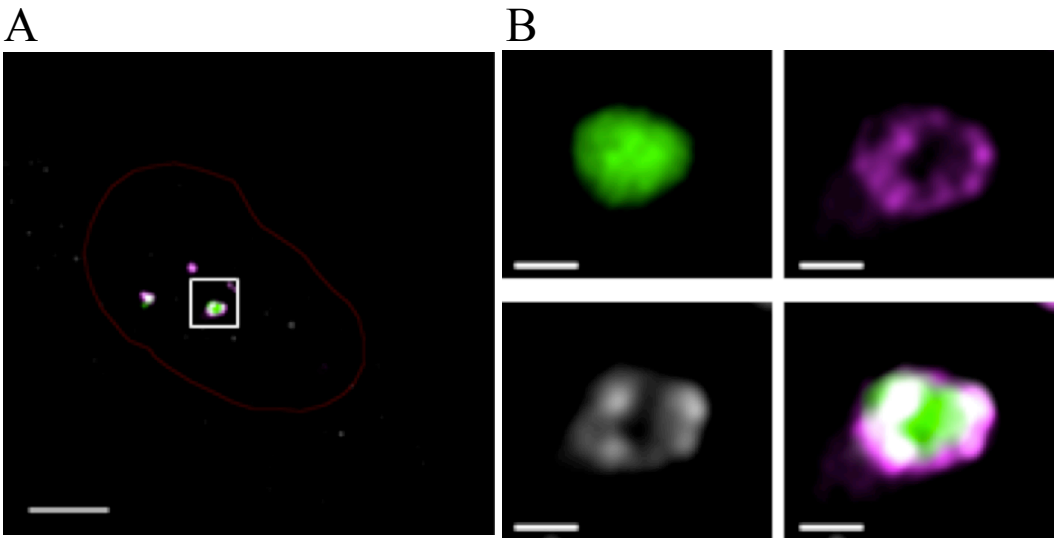

Figure 2: Super-resolution microcopy illuminates the fine structure of the PML body

A, Single plane of a reconstructed structured illumination image (SIM) showing the interaction between PML (magenta), ataxin-1 84Q-GFP (Green), and PMY (gray). Cells were transfected with ataxin 84Q-GFP and subsequently subjected to the ribopuromycylation method (RPM) to detect nascent translation in the nucleus. Scale bar is equal to 5µm. **B**, High resolution SIM image of boxed region in (**A**). Scale bar is equal to 0.6µm.

compartmentalization of function exhibited by nuclear bodies exemplifies the importance for the spatial organization of genes for regulation.

Nuclear crosstalk with the ECM

Historically, the nucleus has been studied as an independent organelle. However, the nucleus is inherently and fundamentally tied to the cell in which it resides. Simply put, nuclear structure and function must respond to the needs of the cell. Cells in tissues exist within 3D microenvironments that have varying mechanical properties; therefore, there must communication from the extracullular matrix (ECM) to the nucleus to regulate particular functions. The linker of the nucleus to the cytoskeleton (LINC) complex directly connects the cytoplasm to the nucleoplasm and provides a platform for communication between nuclear processes and the rest of the cell. The LINC complex is formed by the perinuclear association of nesprin proteins through their KASH domain binding with SUN domain proteins. Nesprins transverse the outer nuclear membrane (ONM) and bind to cytoplasmic actin, intermediate filaments, and microtubules, while SUN domain proteins span the inner nuclear membrane (INM) and bind to the nuclear lamina and nuclear membrane-associated proteins (45). Extra-cellular cues are able to exert their influence on nuclear function through the mechanical force propagation mediated by the cytoskeleton. As such, the physical properties of the nucleus are inextricably linked to cell mechanical phenotypes. For example, it has been shown that perinuclear actin regulates nuclear shape in response to alterations in cell shape, and this regulation is dependent on the LINC complex and lamin A/C (46). Furthermore, actin also mediates lateral compressive forces on the nucleus to coordinate cell and nuclear shape (47). Interestingly, nuclear volume loss caused by nuclear shape change is marked by chromatin

condensation and a decreased cell proliferation rate, indicating that nuclear form and function are directly coupled to extra nuclear forces (47). Given the role that the nuclear lamina plays in establishing genome organization and its direct association with the LINC complex, the extent of nuclear regulation by mechanical forces is becoming increasingly clear. Mechanical force application to the plasma membrane, for instance, alters actin force transmission to the nucleus that causes LINC complex-dependent chromatin decondensation (48). In addition, applying force transmission to cells through integrins via Arg-GlyAsp (RGD) ligand coated magnetic beads, results in the actin-, lamin A/C-, and LINC complex-dependent dissociation of Cajal bodies, showing that nuclear processes, beyond genome organizational patters, can be coupled to external forces (49).

Beyond mechanical force propagation to the nucleus from the plasma membrane, cells can also respond to the mechanical properties of their environment by transmitting biochemical cascades to regulate gene expression. For example, cytoskeletal tension activates the transcriptional activators YAP and TAZ to localize to the nucleus and activate target genes (50). This indicates that there are multiple mechanisms in which nuclear function is coupled to the ECM

Cell polarity as model to study the relationship between nuclear and cellular organization

Cell polarity, which is characterized by the asymmetries in cell morphology and molecular localizations, allows cells to partition function and interact with their varied environments. Cell polarity is essential in a wide variety of cellular processes, ranging from polarized cell division to generate diverse daughter cells during morphogenesis, to the polarized function of cytotoxic T cells when anchoring to target cells (51).

Human epidermal differentiation is an ideal model of both cell polarity and resultant phenotypes that are caused by changes or loss of cell polarity. The human skin is composed of a stratified epithelium. In order to maintain its function as a protective barrier, epidermal differentiation generates constant turnover of terminally differentiated cells (52). The basal layer of the epidermis is comprised of mitotically active progenitor keratinocytes that are attached to the basement membrane by hemidesmosomes (HDs), an integral membrane protein complex that directs adhesion with extra cellular matrix (ECM) components. In the epidermis, HDs anchor the epidermal tissue to the basement membrane zone (BMZ), which separates the connective tissue of the dermis from the epidermis. A central structure of HDs is formed by the heterodimerization of integrins α6 and β4 and association with BPAG1e, which are encoded by the *ITGA6*, *ITGB4*, and *DST* genes, respectively. Proliferation of basal progenitor keratinocytes results in the repression of HD gene expression and initiation of differentiation, which coincides with cellular migration through the stratified epithelium and eventual enucleation to form the protective barrier of the skin (53). Epithelial cells, such as those of the epidermis, are differentiated from other polarized cells by their connective association as a collective group of cells that are adherent to each other as well as the association with the environment outside of the epithelium. The basal progenitor keratinocytes of the epidermis maintain a basal/apical polarity defined by their relationship to extracellular cues, as these cells must bind to different sets of adhesion molecules at discrete surfaces of the plasma membrane. For example, the apical and lateral sides of basal progenitor cells are tightly coupled and anchored to neighboring cells, and therefore are enriched in structures with functions relating to maintaining those cell-cell connections and communications, such as desmosomes, tight junctions, and adherens junctions.

Of course the basal side of the epidermis does not maintain contact with neighboring cells but rather the ECM rich basement membrane zone. As such, the basal side of basal progenitor cells is enriched in HDs so that the epithelium maintains its contact with the basement membrane, which is rich in the HD ligand laminin 332. Importantly, the apical and lateral sides of the plasma membrane are depleted of HDs; therefore, the localization of HDs to the basal side of the plasma membrane in basal progenitor cells of the epidermis represents an example of a cell-polarized structure.

In contrast to the apical/basal polarity exhibited in epithelial cells, migrating cells develop a front/rear polarity with respect to the direction of migration. The most well studied processes that drive polar cell migration involves the initiation of cell protrusions, known as lamellipodia, that are formed by actin polymerization and branching by the Arp 2/3 complex to allow for cell adhesion in the direction of migration (54). In these cells that utilize lamellipodia, Rac and Cdc42, members of the family of Rho GTPases, induce initiation of actin polymerization at the leading edge of the cells. At the rear of the cell, RhoA, another Rho GTPase, induces the formation of focal adhesions and actin stress fibers. During collective cell migration, leader cells coordinate the migration of a group of connected cells, while follower cells remain in contact behind the leader cells; therefore, since follower cells do not contact the ECM they do not exhibit front/rear polarity with respect to actin polymerization (55). Instead, migration of these follower cells depends on the physical interaction through adhesion complexes with the migrating leader cells.

Upon injury, epidermal cells transition from cells that maintain an apical/basal polarity to cells that establish front/rear polarity as migration is induced at the site of the wound (56). Key components that maintain apical/basal polarity in epithelial cells are inhibited, such as the loss of E-cadherins which disrupts adherens junctions in leader cells (57). Importantly, HD genes are normally silent in differentiated suprabasal cells of the epidermis, however, upon injury, suprabasal cells at the leading edge activate the expression of HD genes, such that the components of the HD complex polarize to the front of the cell in the direction of migration (58). Upon closing of the wound, a transition between the front-rear polarity of migrating keratinocytes to the apical basal polarity of "static" keratinocytes in epidermal tissue must be achieved. This is likely coordinated through the detection and interaction of cells at the opposite edge of the wound.

Epidermal differentiation provides an elegant model to study genome organization as it relates to cellular function due to its well-characterized asymmetry. Here, we interrogate the localization of genes that encode components of HDs, and analyze their localization patterns with respect to the location of their protein products in the cells. As basal progenitor cells of the epidermis lose apical/basal polarity with respect HDs upon differentiation, suprabasal cells provide us with an excellent negative control for gene-protein organization relationships. Furthermore, the induction of HD polarity upon wounding in epidermal tissue will allow us to observe the dynamic organization of the genome from an "unpolarized" to a "polarized" state. Here, upon migration induction, follower cells will serve as a negative control for cells that remain unpolarized with respect to HD positioning. Finally, we will investigate the contributions of the physical association of the nuclear membrane with the cytoskeleton on organizing the spatial organization

of genes within the nucleus, and we attempt to provide a functional consequence that results from the relationship between gene and protein localizations.

CHAPTER II

Methods

Materials

Chromosome 2 Paint (XCP 2 Orange, D-0302-100-OR) was from MetaSystems Probes. Wheat germ agglutinin (WGA) conjugated to Alexa 488 (W1161) and WGA conjugated to Alexa 594 (W1162) were from Thermo Fisher Scientific. Restriction Enzymes were purchased from New England BioLabs (Ipswich, MA). All other chemicals were purchased from Sigma-Aldrich (St. Louis, MO), unless otherwise noted.

Sheep anti-Digoxigenin-Fluorescein (11207741910) was from Roche. Rabbit anti-DNP (71-3500) was from ThermoFisher Scientific. AlexaFluor 488 goat anti-rabbit (A11008), AlexaFluor 594 goat anti-rabbit (A11012), AlexaFluor 594 goat anti-mouse (A11005), and AlexaFluor 647 donkey anti-rabbit (A31573), AlexaFluor 594 donkey anti-goat (150132), and Biotin-XX goat anti-rabbit (B2770) were from Invitrogen. AlexaFluor 647 goat anti-biotin (200-602-211) was from Jackson ImmunoResearch. Rabbit anti-Cytokeratin 10 (ab76318), rabbit anti-integrin alpha 6 (ab75737), rabbit anti-pericentrin (ab4448), and mouse anti-RFP (ab65856) were from Abcam. Mouse anti-puromycin (MABE343) was from EMD Millipore. Goat anti-PML (sc-9863) was from Santa Cruz Biotechnology.

C57/BL6 wild type (WT) and *Syne2* KO mice were a generously provided by Angelika Noegel (University of Cologne). Mice were maintained in accordance with local governmental and animal care regulations and all procedures had institutional approval (Washington State University IACUC protocol numbers 04444-006 and 04824-004). All mouse-derived epidermal tissues used in experiments were derived from 21 day-old male or female mice.

Cell Culture and Organotypic Raft Cultures

Human foreskin keratinocytes used for immunoFISH experiments were provided by provided by Laimonis Laimins (Northwestern University). Cells were grown using 1X Defined Keratinocyte-SFM (serum free media) with the included growth supplement (Gibco) and 100 U ml^{-1} penicillin and 100 µg ml^{-1} streptomycin. For scratch wound assay, immortalized keratinocytes expressing the HPV-31 *E6* and *E7* genes were purchased from Northwestern University SDRC Skin Tissue Engineering Core. Cells were grown using Cascade Biologics 154CF media with the included growth supplement (Gibco), as well as 0.07 mM $CaCl_2$, 100 U ml^{-1} penicillin and 100 µg ml^{-1} streptomycin. All cells were maintained at 37 °C in 5% CO_2.

Human foreskin keratinocytes used for the generation of raft cultures were isolated from neonatal foreskin tissue obtained from anonymous donors by the Northwestern University Skin Disease Research Center (SDRC) and grown as described previously (59). Raft cultures were generated by the Northwestern University SDRC Skin Tissue Engineering Core. To generate organotypic raft cultures, keratinocytes were seeded onto collagen plugs

containing J2-3T3 fibroblasts and grown in an air-liquid interface as described previously (60, 61). For wound assays, organotypic raft cultures were generated as described and wounded with a 4mm punch biopsy tool on day 7. At the time of wounding, another collagen plug was placed below the wounded raft. Raft cultures were then fixed after 2-5 days post-wounding to allow for migration into the wound site.

Vectors encoding RFP-KASH and RFP-KASHΔL in the pm-RFP-C1 backbone were kindly provided by G.W. Gant Luxton (University of Minnesota). These vectors were used to amplify RFP-KASH and RFP-KASHΔL by PCR with XbaI overhangs and then each sub-cloned into the 3rd generation commercial lentiviral vector CD510B-1 (System Biosciences, Palo Alto, CA, USA) into the XbaI restriction site. Lentivirus generation and transductions were performed by the Northwestern University SDRC DNA/RNA Delivery Core. To stably express RFP-KASH, the VSVG pseudotyped lentivirus expressing either RFP-KASH or RFP was generated as described (62) using 293T packaging cells (Gene Hunter Corporation) and 2nd generation packaging vectors psPAX2 and pMD2.G (Addgene). The CD510B-1 RFP expressing virus was used as a control. Since lentiviral infection efficacy in primary normal human keratinocytes was > 90%, the bulk cell populations, but not individual stably infected cell clones, were used to establish the stable cell lines expressing RFP-KASH, RFP-KASHΔL, or RFP control. If required, the stable cell lines were maintained in the presence of 4 μg/ml puromycin. These stable cell lines were then used to generate organotypic raft cultures, as described previously.

Microscopy

Unless otherwise noted, images were acquired on a Nikon A1R laser scanning confocal microscope equipped with photomultiplier tubes (for the 405 and 638 channels) and GaAsP detectors (for the 488 and 561 channels). Images were acquired using the Nikon Elements software.

H&E staining

Paraffin-embedded tissue sections on slides were baked upright for 15 mins at 60°C. Slides were then submerged in Sub-X Clearing Agent (Leica Biosystems) 3 times for 2 mins each. Slides were then subjected to the following ethanol washes: two times in 100% ethanol for 2 mins each, two times in 95% ethanol for 2 mins each, and 1 time in 70% ethanol for 2 mins. Slides were then incubated with SelecTech Hematoxylin 560 (Leica Biosystems) for 6 mins. Slides were then washed with deionized water 4 times for 1 min each. Slides were then incubated in an acid alcohol solution (made from 69.8 mL isopropyl alcohol, 29.7 mL dH20, and 0.5 mL concentrated HCl) for 1 min, SelecTech Blue Buffer 8 (Leica Biosysems) for 1 min, 95% ethanol 2 times for 2 mins each, and 100% ethanol 2 times for 2 mins each. Slides were submerged in Sub-X Clearing Agent 4 times for 2 mins each and then mounted using Permount (Fisher Scientific). Slides were imaged using a Nuance spectral imaging system (Cambridge Research & Instrumentation, Inc.) on a Zeiss Axioskop upright microscope.

Scratch wound assay

Immortalized human epidermal keratinocytes were transduced with the VSVG pseudotyped lentivirus expressing RFP-KASH as described above. WT and RFP KASH-expressing cells were plated onto 96-well plates and allowed to adhere for 24 hours. Confluent wells were scratched using a WoundMaker tool (Essen Biosciences) followed by 3 washes in normal media. Live cells were imaged in 3 hour intervals for 24 hours using the Incucyte S3 Live-Cell Analysis System (Essen Biosciences). Images were analyzed using ImageJ. Percent wound closure for each timepoint was measured as 1-(area of *x*hr timepoint/area of 0hr timepoint).

DNA FISH probe preparation

Bacterial Artificial Chromosomes (BACs) containing our genes of interest were labeled by nick translation with DIG-11-dUTP (11558706910, Roche) or DNP-11-dUTP (NEL551001EA, PerkinElmer) using the Roche Nick Translation Mix (11745808910) according to the manufacturer's instructions. All of the BACs used in this study where acquired from the BACPAC Resources Center at the Children's Hospital Oakland Research Institute and are listed in Table 2. After nick translation, the probe mixture was heat inactivated at 65°C for 10 minutes. Unincorporated nucleotides were removed using the illustra ProbeQuant G-50 Micro Columns (GE Healthcare).

For each coverslip of cells, a probe mixture containing 5µl of the nick translated probe, 1µl of 1µg/µl cot1DNA (15279011, Invitrogen), and 5µL of 1µg/µl salmon sperm DNA (15632011, Invitrogen) was ethanol precipitated. For each tissue section, a probe mixture of 10µl of the nick

translated probe, 2µl of 1µg/µl cot1DNA, and 5µL of 1µg/µl salmon sperm DNA was used instead. The dried pellet was resuspended in 10µl of hybridization buffer (10% dextran sulfate in 50% Formamide/2X SSC). The probe was then mixed in a rotating heat block at 37°C for at least 1hr before hybridization.

3D DNA immunoFISH on cultured cells

Cells grown on coverslips were fixed with 4% formaldehyde for 10 minutes followed by 3 washes with PBS for 5 minutes each. Cells were then permeabilized with 0.5%Triton X-100 in PBS for 15 minutes, blocked in 4% BSA in PBST (0.1% Triton X-100 in PBS) for 10 minutes, and then incubated with the primary antibody at 37°C for 1 hour. Cells were then washed in PBST twice for 5 minutes each and then incubated with a second biotinylated antibody at 37°C for 45 minutes. Following antibody incubation, cells were washed twice with PBS for 5 minutes each, post-fixed in 1% formaldehyde in PBS for 10 mins, incubated in 0.1N HCl for 8 minutes, permeabilized with 0.5% Triton X-100 in PBS for 5 minutes, and then incubated in 20% glycerol in PBS for 45 mins-2 hrs. Cells were then subjected to four rounds of freeze-thaws by submerging the coverslips in liquid nitrogen and allowing the coverslips to thaw in 20% glycerol. Cells were then washed in 2X SSC for 5 minutes and stored in a 50% formamide/2X SSC solution for at least 24 hours. Probe (see section on probe preparation) in hybridization solution was placed onto a slide and coverslips were then placed onto the probe and sealed with rubber cement, followed by denaturation at 75°C for 5 minutes, and then incubated in a humid chamber at 37°C overnight. Following probe incubation, rubber cement was removed, and cells were washed in 2X SSC three times for 5 mins each at 37°C with gentle shaking and then 0.1X SSC at 60°C three times for 5 mins each with gentle shaking. Cells were then rinsed in 4X

SSC/0.2% Tween-20 in PBS, and then blocked in 4X SSC/0.2% Tween-20/4% BSA for 45 mins at 37°C. Cells were then incubated with antibodies diluted in 4X SSC/0.2% Tween-20/1% BSA for 45 mins at 37°C. If needed, cells were then washed with 4X SSC/0.2% Tween followed by another second round of antibody incubation. Cells were then washed twice with 4X SSC/0.2% Tween-20 and mounted in Prolong Diamond with DAPI (ThermoFisher).

3D DNA immunoFISH on raft cultures and tissue sections

Formalin-fixed and paraffin-embedded tissues on slides were deparafinized by immersing 3 times in Hemo-De (Scientific Safety Solvents) for 10 minutes each. Slides were then subjected to the following immsersions: 2 times for 15 mins each in 100% ethanol, 5 mins in 95% ethanol, 5 mins in 70% ethanol, 5 mins in 50% ethanol, and 5 mins in dH20. Slides were then immersed in Antigen Retrieval buffer (10mM Tris, 1mM EDTA, pH9) in a coplin jar at 99°C for 1 hr, and then let cool by wrapping the coplin jar in a wet paper towel for 10 mins. Slides were rinsed with dH20, followed by a rinse with Wash Buffer (0.05M Tris-HCl, 1.5M NaCl, 0.5% Tween-20, pH 7.6), and then incubated with 10% donkey or 10% goat serum in Wash Buffer for 1 hr. Slides were then incubated with primary antibodies with 1% serum/Wash Buffer overnight at 4°C. Following antibody incubation, slides were washed in Wash Buffer 3 times for 10 minutes each, incubated with a secondary biotinylated antibody at 37°C for 1 hr in 1% serum in Wash Buffer, and then washed again 3 times for 10 minutes each in Wash Buffer. Slides were then rinsed in PBS, fixed in 4% formaldehyde in PBS for 10 minutes, and washed in PBS twice for 5 mins. Slides were then permeabilized with 0.5% Triton X-100 in PBS for 30 mins, washed with PBS, and incubated in 50% Formamide/50% 4X SSC o/n. Probes were placed on the tissue and a coverslip

placed over the probe. Sections were incubated with the probe at RT for 2 hrs, and then denatured at 85°C for 8 mins. Slides were placed in a humid chamber to hybridize at 37°C for 2 days. After hybridization, the coverslips were removed and slides were washed 3 times for 10 mins with 2X SSC at 37°C and then once with 0.1X SSC at 60°C. Tissue sections were blocked with 4% BSA in 4X SSC/0.2% Tween-20 for 15 mins and then incubated with antibodies diluted in 1% BSA in 4X SSC/0.2% Tween-20 for 1hr 20 mins at 37°C. Slides were then washed 3 times for 5 mins with 4X SSC/0.2% Tween-20. If needed, a second round of antibody incubation was performed followed by another round of washing. Sections were mounted with Prolong Diamond with DAPI.

RNA FISH on raft cultures

To detect single mRNA particles, custom Stellaris FISH probes were designed against the exons of *ITGB4* using the Stellaris FISH probe designer (Biosearch Technologies). The exact probe sequences are listed in Table 3. Raft cultures were hybridized with the *ITGB4* exonic probe set labeled with Quasar 670 following the manufacturer's instructions for formalin-fixed, paraffin-embedded (FFPE) tissues, with the exception that Hemo-De (Scientific Safety Solvents) was used instead of xylene to defarrafinize the tissues. RNA FISH images were acquired as widefield Z-stacks of 0.2µm using a Nikon Ti-E inverted microscope equipped with a Lumen Dynamics XT120L LED light source and the appropriate filter sets. To control for background, slides were images in an empty channel using the same exposure and illumination settings as those used to image the RNA FISH signal. Detection of mRNA particles was performed using FISHquant according to the user-manual (63). To obtain the normalized distribution of mRNA particles relative to the basement membrane, each cell

border was traced in FIJI using the WGA signal as a reference and saved as a region of interest (ROI). Using the image coordinates for each mRNA particle obtained using FISHquant, as mentioned previously, we used an in-house MATLAB package to find the normalized distribution of each mRNA spot relative to the cell boundary nearest and furthest to the basement membrane.

RNA FISH on cultured myotubes

To detect nascent transcripts, custom Stellaris FISH probes were designed against the introns of myogenin (MYOG; NM_002479.5) by utilizing the Stellaris FISH probe designer (Biosearch Technologies). The exact probe sequences can be found in Table 4. Cells were hybridized with the MYOG intronic Stellaris FISH probe set labeled with Quasar 570 (Biosearch Technologies) following the manufacturer's instructions for adherent cells. Slides were imaged using a Leica DMI6000 B microscope equipped with a Lumen 200 illumination system (Prior Scientific), a PLAN APO 63X 1.4 NA oil immersion objective lens, and a CoolSNAP HQ2 CCD camera (Photometrics). We used the A4 and TX2 filtercubes from Leica to image DAPI and Quasar 570, respectively. Images were acquired with 0.2 μm Z steps in each channel using a motorized stage controlled by the Leica Application Suite Advanced Fluorescence software. To quantify the relative levels of bi-allelic nascent transcription, we used FIJI to obtain the maximum pixel value for two intronic signals within the same nucleus and subtracted these values to obtain our delta value**.** This method of quantification controls for variability of signal intensities between cells and images.

Real-Time PCR

Total RNAs from raft cultures were isolated using Trizol Reagent (Invitrogen). cDNA was made using Superscript IV Reverse Transcriptase (Invitrogen) with Oligo $d(T)_{20}$ primers following the manufacterer's instructions. qPCR was performed using a Roche LightCycler 480 Real-Time PCR system and the LightCycler 480 SYBR Green I Master mix (Roche). Samples were quantified relative to GAPDH. Primers used in qPCR analysis are listed in Table 5.

Structured illumination microscopy of PML bodies

Nuclear ribopuromycylation method was performed as described in (39). Briefly, transfected IMR-90 cells seeded on coverslips were incubated for 18-24 hours prior to RPM. Cells were incubated for 5 minutes in labeling media (complete MEM alpha with 208uM emetine and 91uM puromycin) then washed with cold PBS. Permeabilization was performed for 5 minutes in permeabilization buffer with NP-40 (50mM Tris-HCl,150mM NaCl, EDTA-free protease inhibitors, and 1% NP-40) and washed with permeabilization buffer without NP-40. Cells were then fixed in 4% formaldehyde. Prior to primary antibody incubation, cells were blocked in staining buffer (0.05% saponin, 10mM glycine, 5% FBS, in PBS). Primary and secondary antibodies were added to coverslips and incubated at 37°C for 1 hour or 45 minutes, respectively before washing and incubating in Hoescht (1:5000) for minutes. Slides were mounted in Pro-Long Gold Anti-Fade (Invitrogen). Images were acquired on a Nikon N-SIM microscope with a 100X 1.49 NA Plan Apo TIRF objective lens (Nikon) and an Andor DU-897 EMCCD camera using 405nm, 488nm, 561nm, and 640nm diode lasers. 3D-SIM stacks were acquired using five phases and three rotations for a total of 15 widefield images per plane, and images were reconstructed using Nikon Elements software.

CHAPTER III

Results

Gene polarity in keratinocytes

The nucleus is inextricably tied to the cell in which it resides. To test the hypothesis that nuclear organization is related to the cellular localization of proteins, we analyzed epidermal differentiation due to its well-characterized asymmetry (52, 64). As previously described, the basal progenitor keratinocytes express HDs, which are locally polarized to the basal portion of the cells adjacent to the basement membrane. Upon differentiation and movement through the epithelial layers, HD expression is lost and, of course, the protein is not polarized.

To serve as a model of epidermal differentiation we used three-dimensional (3D) in vitro organotypic raft cultures (hereafter referred to as raft cultures) in which primary keratinocytes are grown on a collagen plug that mimics the basement membrane. These keratinocytes are induced to differentiate and form a stratified epithelium (65). Immunofluorescence (IF) staining of thin sections from raft cultures with an antibody to keratin 10 (K10), a marker of differentiation, illustrates that the most basal layer of cells is K10-negative, and thus represents the progenitor keratinocytes of the epidermis (Figure 3A).

To test whether the formation of the asymmetrically localized HD complexes relate to nuclear organization, we performed 3D fluorescence *in situ* hybridization (3D-FISH) using bacterial artificial chromosomes (BACs) that cover the HD genes *ITGA6*, *ITGB4*, and *DST* to analyze

their spatial positions within the nucleus. We devised an analytical method to determine apical/basal position of the genes within the nucleus relative to their tendency to be positioned towards or away the basement membrane (Figure 3B). In these quantifications, we assigned a value of *1* to represent the position in the nucleus that is most proximal to the basement membrane and the value of *-1* to represent the position in the nucleus that is most distal to the basement membrane. Zero *0* represents the position in the nucleus that is exactly equal distance from the most proximal and most distal positions relative to the basement membrane. This method of quantification allows us to control for nuclear size and shape that may vary between individual cells. In support of our hypothesis, we observe a significant polarization of HD genes toward the basal side of the nucleus specifically in the progenitor keratinocytes that express them, as opposed to the differentiating suprabasal cells in which they are silenced (Figure 3C). Desmoplakin is a cell adhesion protein that localizes to the plasma membrane and is expressed in both basal and suprabasal cells. In basal cells, however, desmoplakin is excluded from the basal side of the plasma membrane. We observe that the gene encoding desmoplakin *DSP*, and the housekeeping gene *GAPDH* do not demonstrate polarized gene positioning relative to the basement membrane (Figure 3C).

In order to determine the physiological relevance of our system, we corroborated our findings in normal human skin tissue (Figure 4A). Here, we find that the nuclear distribution of *ITGA6*, but not *GAPDH*, is skewed towards the basal side, proximal to the basement membrane, and that this distribution significantly differs when compared to the distribution of the gene in suprabasal cells (Figure 4B-C).

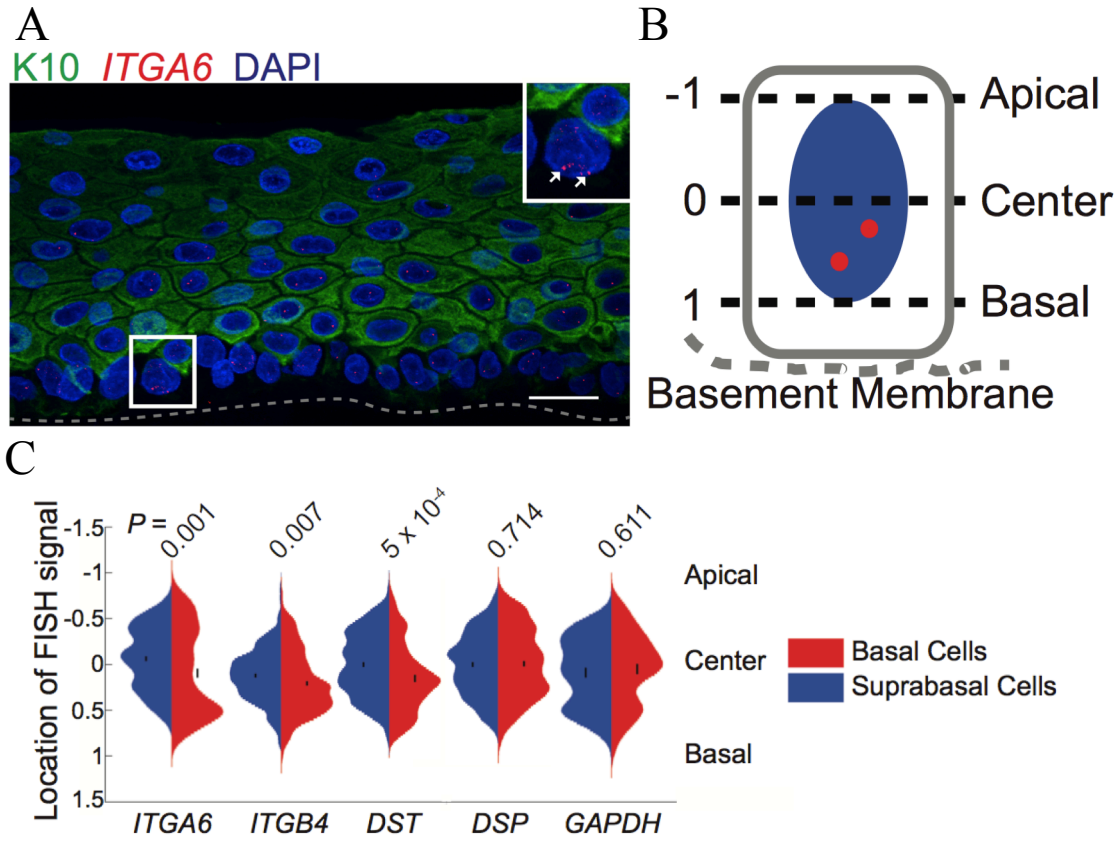

Figure 3: HD genes are polarized in basal cells of organotypic raft cultures

A, ImmunoFISH image showing the position of an HD gene, *ITGA6* (red), relative to the basement membrane (dotted line), in a thin section of a raft culture. K10 (green) is used as a marker of differentiation and DAPI (blue) is used as a nuclear counterstain. Scale bar=20 μm. **B**, Schematic of analysis method to examine gene positioning relative to the basement membrane. **C**, Normalized gene positions (for genes indicated) relative to the basement membrane in raft cultures for basal (red) and suprabasal (blue) cells. Results represent pooled data from 3 raft

(Figure 3 cont.)

cultures (biological replicates). For *ITGA6*, N = 113 (basal cells) and 116 (suprabasal cells) loci. For *ITGB4*, N = 208 (basal cells) and 209 (suprabasal cells) loci. For DST, N = 100 (basal cells) and 195 (suprabasal cells) loci. For *DSP*, N = 164 (basal cells) and 199 (suprabasal cells) loci. For *GAPDH*, N = 51 (basal cells) and 50 (suprabasal cells) loci. Violin plots were chosen to depict all gene localization analyses as they allow for evaluation of the full distribution of data. Bars represent the standard error of the mean and *P* values derived from two-tailed Student's t-test.

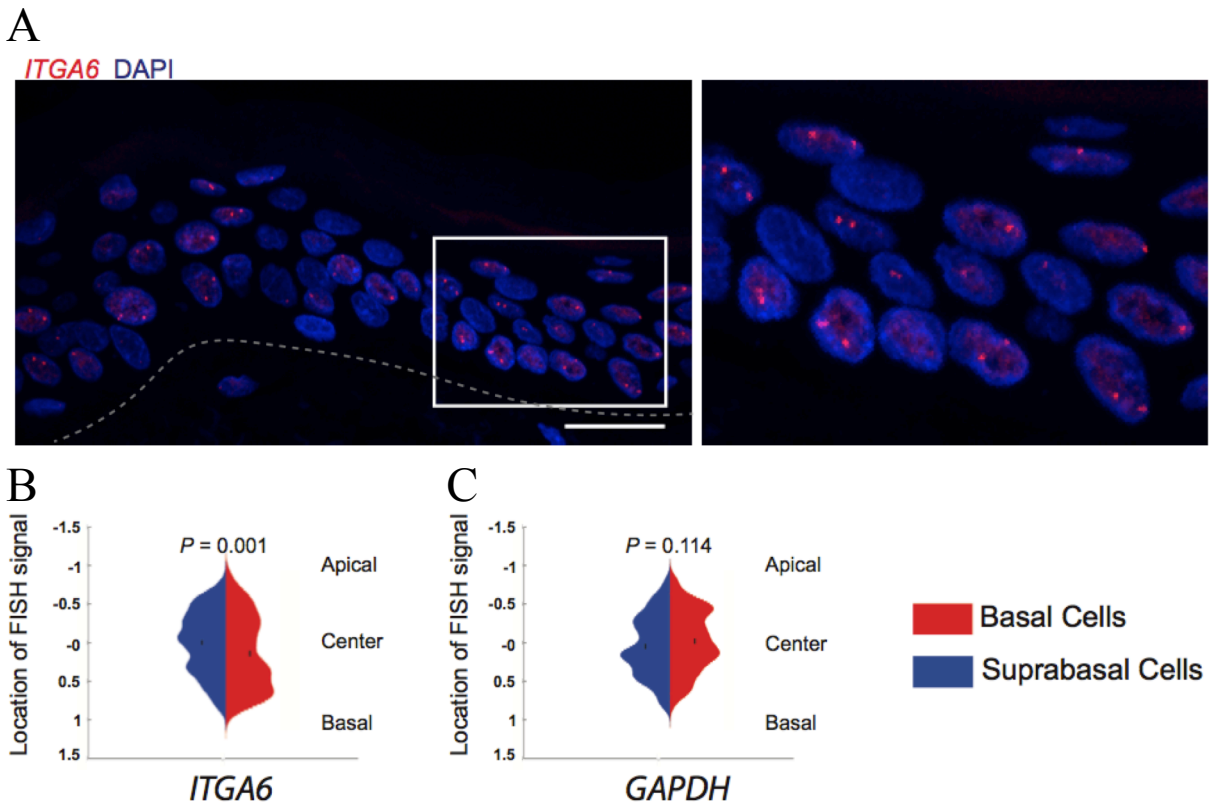

Figure 4: *ITGA6* is polarized towards the basement membrane in basal cells of human skin

A, 3D FISH image of a normal human skin sample showing the position of *ITGA6* (red) relative to the basement membrane (dotted line). DAPI (blue) is used as a nuclear counterstain. Scale bar=20 µm. Normalized gene positions of **B** *ITGA6* and **C** GAPDH in basal (red) and suprabasal (blue) cells. For (**B**) N = 170 loci for basal cels and N = 252 loci for suprabasal cells. For (**C**) N = 141 loci for basal cells and N = 178 loci for suprabasal cells. Bars represent the standard error of the mean and *P* values derived from two-tailed Student's t-test.

Upon IF staining for integrin α6 in raft cultures, we noticed variability with regards to the intensity of protein stain in different areas of the tissue (Figure 5A). To test whether the nuclear positioning of HD genes correlates with HD protein expression in those cells, we analyzed the localization of HD genes in basal cells in cells that had a high degree of protein polarity and cells that had a low degree of protein polarity (Figure 5A). We found that the nuclear distribution of HD gene positioning within individual basal cell nuclei significantly correlates with HD protein expression in those cells (Figure 5B); i.e. the degree of gene polarization is more pronounced in basal progenitor cells when taking into account defined protein localization. In cultured keratinocytes grow in colonies on a 2D monolayer, cells at the edge of the colony often exhibit integrin α6 protein polarity towards the colony edge (Figure 6A). We tested whether an HD gene, *ITGA6*, could be positioned towards the colony edge in cells that exhibit integrin α6 protein polarity towards the colony edge. We find that in colony edge cells demonstrating integrin α6 protein polarity, *ITGA6* loci tend to be positioned towards the adjacent nuclear edge in those cells (Figure 6B). Furthermore, there is a significant difference in the distribution of the positioning of the loci when compared to the distribution of the positions in colony edge cells that do not express integrin α6 protein polarity (Figure 6B).

The relationship between the ITGA6 locus and its chromosome territory

The location of a gene within its chromosome territory (CT) can have a significant impact on its regulation. For example, certain gene clusters have been shown to loop away from their CT upon activation, and active genes have been known to localize to the periphery of their CT, presumably to be positioned near transcription factories that reside in the interchromosomal space (66). Here, we sought to examine the relationship between one HD gene, *ITGA6*, and its

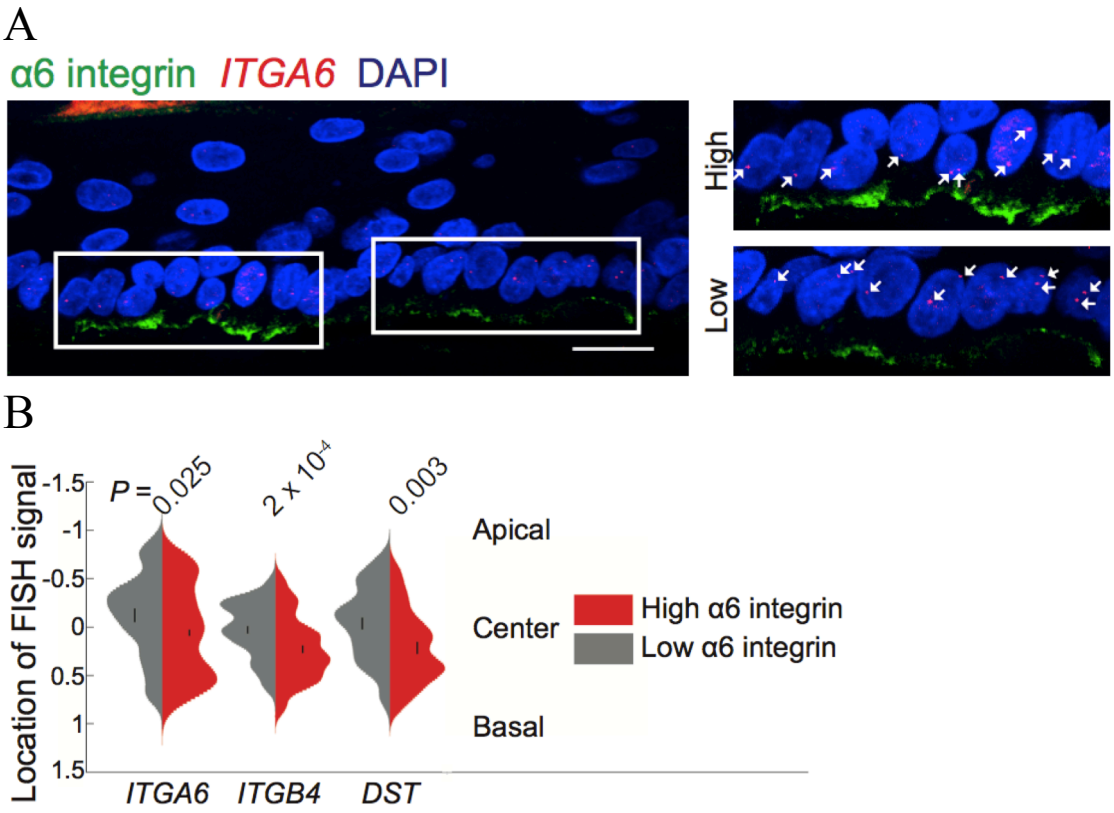

Figure 5: HD gene polarization is correlated with the degree of HD protein polarization in raft cultures

A, ImmunoFISH images showing the position of an HD gene, *ITGA6* (red), in raft cultures. Inserts highlight areas of the raft culture that show both high and low levels of α6 integrin protein (green) localization. DAPI (blue) is used as a nuclear counterstain. Scale bar=20 µm. **B,** Normalized gene positions relative to the basement membrane in areas of the raft culture that exhibit high (red) and low (gray) levels of α6 integrin protein. For *ITGA6*, N = 240 (high α6) and 37 (low α6) loci. For *ITGB4*, N = 74 (high α6) and 59 (low α6) loci. For *DST*, N = 35 (high α6) and 37 (low α6) loci. Bars represent the standard error of the mean and *P* values derived from

(Figure 5 cont.)

two-tailed Student's t-test. Results represent pooled data from 3 raft cultures (biological replicates).

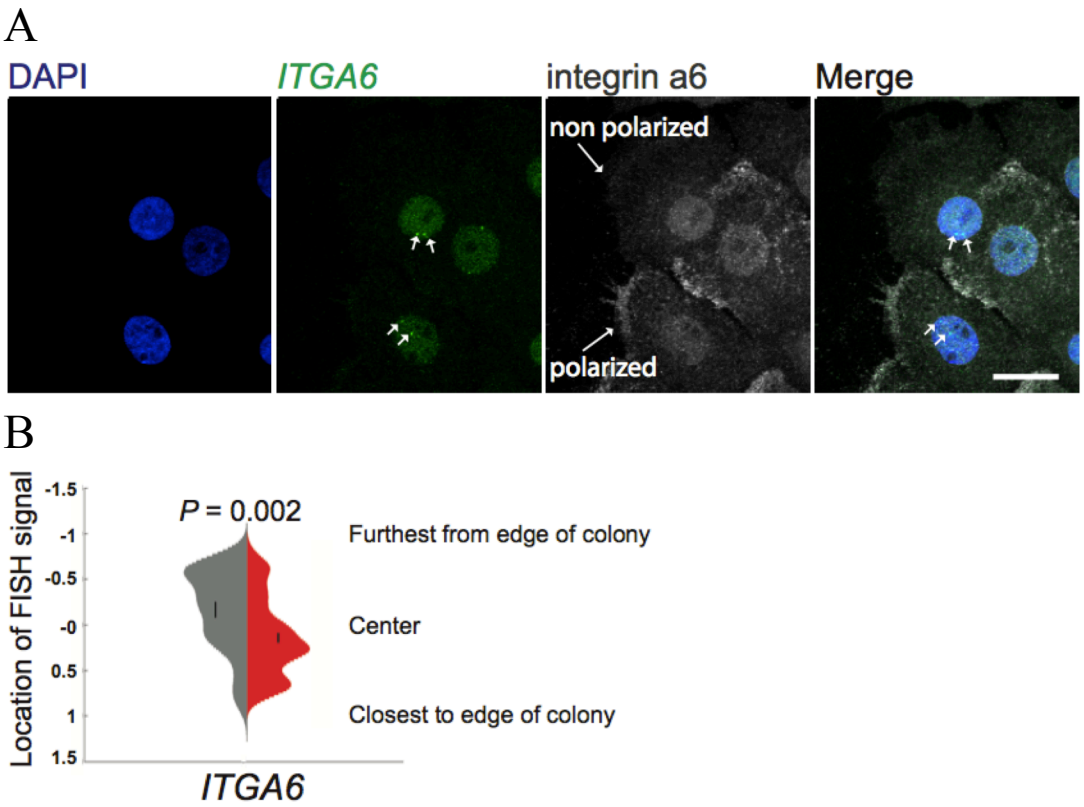

Figure 6: HD gene polarization is correlated with the degree of HD protein polarization in single cells

A, ImmunoFISH image of cultures keratinocytes highlighting the position of *ITGA6* (green) relative to the variability of intergrin α6 protein (gray). Arrows highlight two cells that show the presence or absence of intergrin α6 protein towards the colony edge of the cell. DAPI (blue) is used as a nuclear counterstain. Small arrows highlight FISH signal localization. Large arrows highlight the lack of (top cell) or presence of (bottom cell) intergrin α6 protein polarity. Scale bar=20 μm. **B**, Normalized position of *ITGA6* relative to the cell colony edge in cells that exhibit a high (red) or low (gray) level of α6 integrin protein localization. N = 24 loci for low α6

(Figure 6 cont.)

levels (gray) and N = 66 loci for high α6 levels (red). Bars represent standard error of the mean.and *P* value derived from a two-tailed Student's t-test.

CT on which it resides, HSA2. When we perform 3D FISH with probes to *ITGA6* and a whole chromosome paint to HSA2 (Figure 7A), we find that the gene loci have a significant propensity to be positioned toward the basal side of the HSA2 CT in progenitor keratinocytes when compared to suprabasal cells (Figure 7B-C). Analysis of the radial positioning of *ITGA6* relative to HSA2 or to the nuclear periphery itself reveal a significant propensity for the peripheral positioning of the locus in basal progenitor cells (Figure 7D-F). Taken together, these results elaborate the deterministic relationship between gene and protein polarity, and suggest a previously unconsidered mechanism for establishing asymmetry in eukaryotic cells.

Gene polarity in wound healing

In addition to the polarized distribution of HD proteins in basal progenitor keratinocytes of the epidermis, they are also expressed and asymmetrically localized toward the leading edge in wounded and migrating keratinocytes (58). To test whether HD genes polarize to the leading edge of nuclei in migrating cells, we performed a wound assay in raft cultures using a 4mm punch biopsy. As previously reported, we observe integrin α6 protein polarization 2-5 days after wounding, but not in a raft culture fixed immediately after wounding (Figure 8). We performed 3D FISH to assay the localization of HD genes *ITGA6*, *ITGB4*, and *DST* with respect to the leading edge in leading-edge cells and follower cells (Figure 9 A-B). We find that HD genes localize towards the leading edge side of the nuclei in leasing edge cells where these genes are induced after wounding, but not in follower cells where they remain transcriptionally inactive. (Figure 9C).

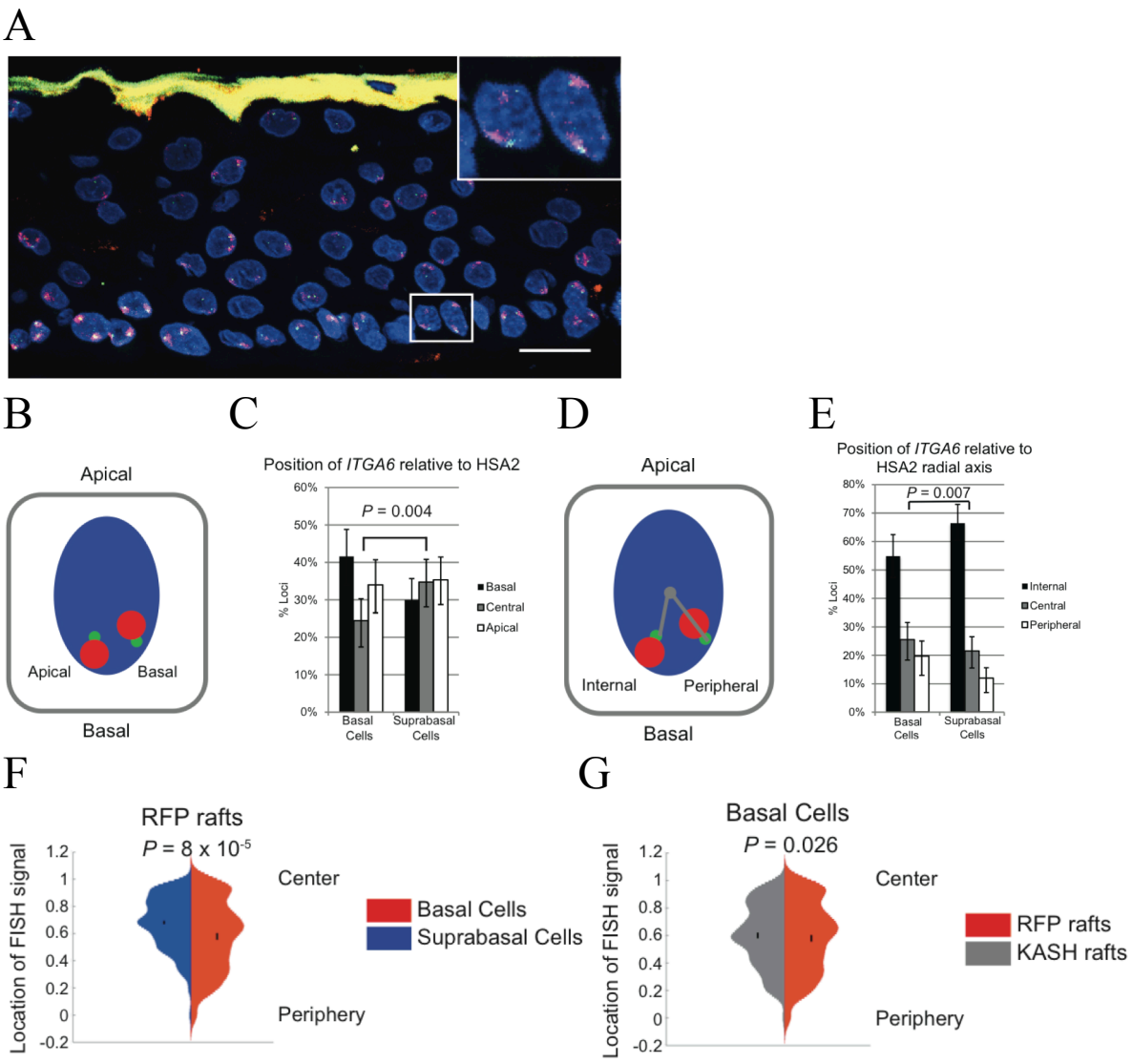

Figure 7: *ITGA6* is positioned towards the basal side of HSA2 in basal cells of raft cultures

A, Combined FISH and chromosome paint image highlighting the position of *ITGA6* (green) relative to HSA2 (red). DAPI (blue) is used as a nuclear counterstain. Scale bar=20 µm. **B**, Schematic showing the possible positions of measurement of *ITGA6* relative to HSA2. **C**, Quantification of *ITGA6* position relative to HSA2 in basal and suprabasal cells of WT raft cultures. N=262 loci for basal cells and N=334 loci for suprabasal cells. **D**, Schematic showing the possible radial orientation of *ITGA6* relative to HSA2 within the nucleus. **E**, Quantification

(Figure 7 cont.)

of the radial position of *ITGA6* relative to HSA2 in basal and suprabasal cells of WT raft cultures. N=259 loci for basal cells and N=334 loci for suprabasal cells. **F**, Radial position of *ITGA6* within the nuclei of basal (red) and suprabasal (blue) of RFP-expressing rafts. N=130 loci for basal cells and N=283 loci for suprabasal cells. **G**, Radial position of *ITGA6* within the basal cells of RFP-expressing (red) and KASH-expressing (gray) rafts. N=130 loci for RFP rafts and N=130 loci for KASH rafts. For (**C**) and (**E**), error bars represent 95% confidence intervals and *P* value derived from multinomial probability. For (**F**) and (**G**), error bars represent standard error of the mean and *P* value derived from two-tailed Student's t-test.

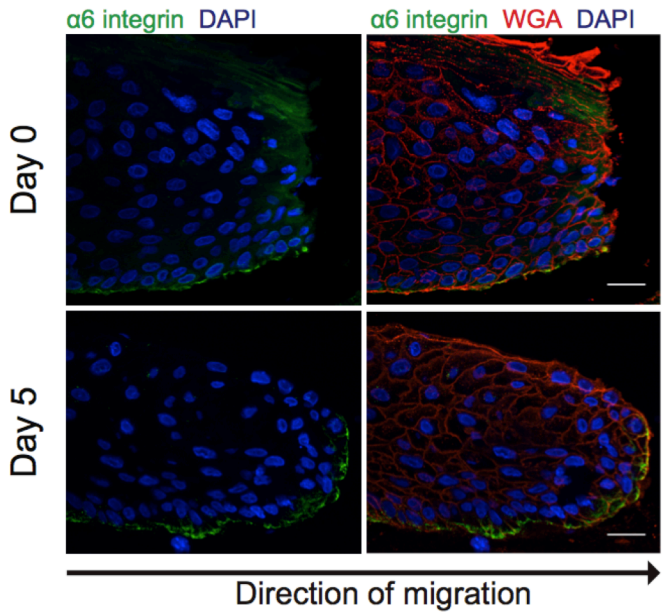

Figure 8: **Integrin α6 protein is dynamically recruited and polarized towards the wound site in leading edge cells in raft cultures**

Immunofluorescence image showing the localization of α6 integrin protein (green) relative to the direction of migration. DAPI (blue) us used as a nuclear counterstain and WGA (red) is used to demarcate cell membranes. Scale bar=20 μm.

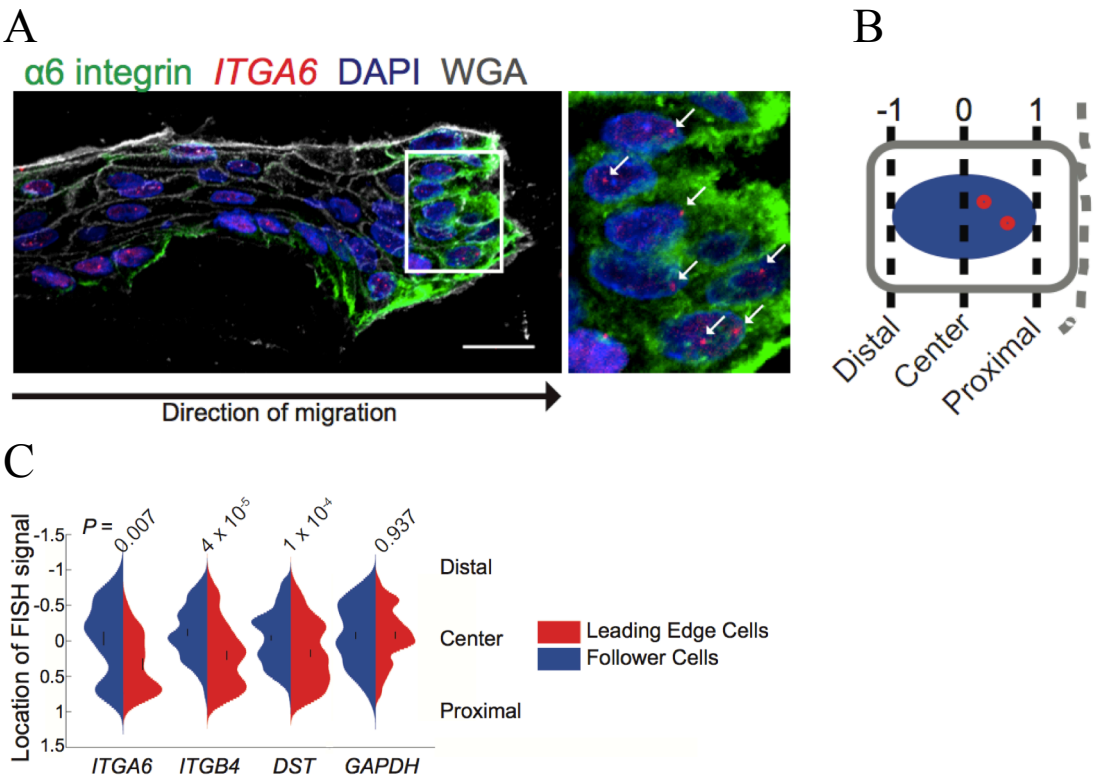

Figure 9: **HD genes dynamically polarize towards the leading edge in wounded raft cultures**

A, ImmunoFISH image of a wounded raft culture showing the position of *ITGA6* (red) and α6 integrin protein (green) relative to the leading edge. DAPI (blue) is used as a nuclear counterstain and WGA (gray) demarcates cell membranes. **B**, Schematic of normalization method to examine gene positioning relative to the leading edge (dotted line). **C,** Normalized gene positions relative to the leading edge in leading edge cells (red) and in follower cells (blue). For *ITGA6*, N = 22 (leading cells) and 27 (follower cells) loci. For *ITGB4*, N = 52 (leading cells) and 62 (follower cells) loci. For *DST*, N = 80 (leading cells) and 133 (follower cells) loci. Results represent pooled data from 4 wounded rafts (biological replicates). All arrows in image inserts highlight FISH signal localization. Scale bar is equal to 20 µm. Error bars represent the standard error of the mean and *P* values derived from two-tailed Student's t-test.

The effect of substrate detachment on gene polarity

The nucleus is indirectly connected the ECM via the cytoskeletal interaction with integrins (67). To elucidate the relationship between gene polarity and the connection of basal progenitor keratinocytes to the ECM, we performed a detachment assay in which raft cultures are physically removed from the underlying substrate (collagen plug) and floated in media over a set time course. We monitored the effect of raft detachment on tissue organization through IF staining with an antibody to K10 to distinguish basal progenitor keratinocytes (K10-negative) to differentiated cells (K10-positive) (Figure 11A). After 8 hours of detachment, undifferentiated K10-negative cells that are restricted to the most basal layer of raft cultures at 15 minutes and 2 hours post-detachment, are now found in more apical layers of the raft (Figure 11A). By 16 hours post-detachment, 'pearls' of K10-negative cells are observed throughout the tissue as previously reported (68). Importantly, we observe similar protein reorganization when detecting integrin α6 localization by IF after raft detachment (Figure 10). 3D FISH analysis (Figure 11A) reveals polarized HD gene positioning K10-negative cells 15 minutes after detachment when compared to K10-positive cells, indicating that the mechanical stress of raft detachment does not influence gene localization (Figure 11B). When compared to K10-positive cells, polarized gene positioning of *ITGA6* and *ITGB4* in K10-negative cells is lost 2 hours post-detachment and polarized gene positioning of *DST* is lost by 8-hours in K10 negative cells (Figure 11B). A comparison of the later timepoints of K10-negative cells to the earliest 15 minute timepoint reveals a similar pattern of dispelled polarization (Figure 11C). These results indicate that gene polarity is related to the attachment of basal progenitor keratinocytes to the underlying collagen

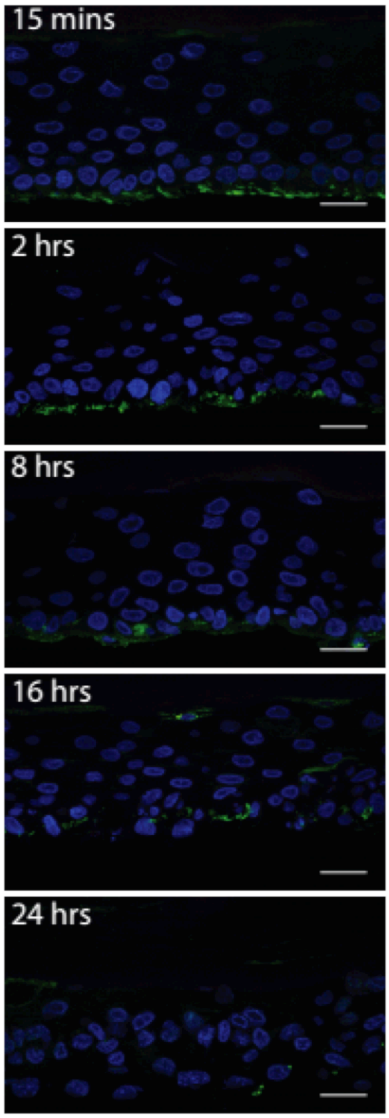

Figure 10: **Integrin α6 protein localization is lost after raft detachment from its underlying substrate**

Immunofluorescence image showing the localization of α6 integrin protein (green) during a time course post-detachment from the basement membrane. DAPI (blue) is used as a nuclear counterstain. Scale bar=20 μm.

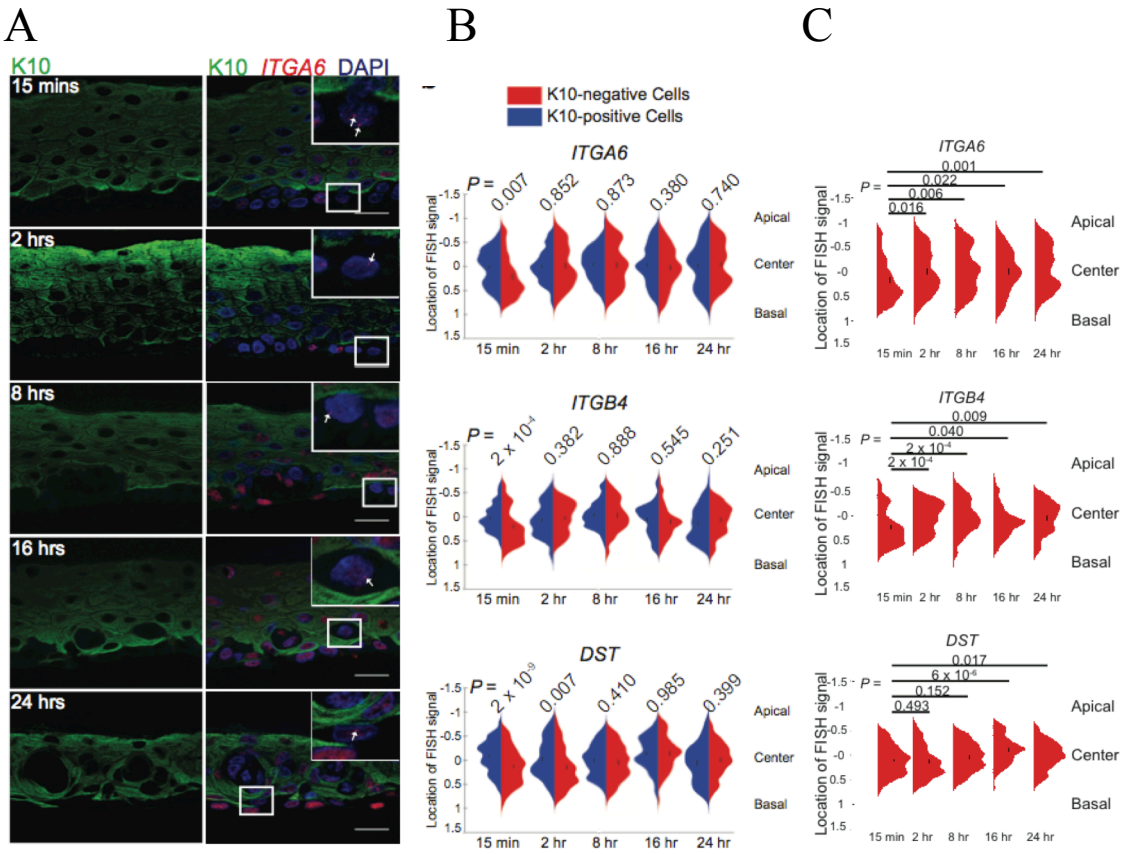

Figure 11: HD gene polarity requires attachment to the basement membrane

A, ImmunoFISH image showing the position of an HD gene, *ITGA6* (red), in raft cultures over a timecourse after detachment from the basement membrane. DAPI (blue) is used as a nuclear counterstain and K10 (green) is used as a marker of differentiated cells. Scale bar is equal to 20 μm **B,** Normalized gene positions relative to the basement membrane after detachment in raft cultures for basal (red) and suprabasal (blue) cells. **C,** Comparison of normalized positions of HD genes in the basal cells of raft cultures during a time-course post-detachment. . For all experiments, bars represent standard error of the mean and *P* values derived from two-tailed

(Figure 11 cont.)

Student's t-test. For all data, results are pooled from 2 detached rafts each (biological replicates). For all data, N values are listed in Table 1.

plug, and since polarized protein localization is also lost over the time course, that gene and protein polarity are inextricably linked.

The role of the LINC complex in maintaining HD gene polarity

HDs are associated with cytoplasmic intermediate filaments, comprised of keratins in the epidermis, which in turn interact with the LINC complex (45, 69-71). Given that the LINC complex exerts its effect on nuclear function after cytoskeletal exertion (72), we hypothesized that the LINC complex functions to maintain HD gene polarity in the basal progenitor cells of raft cultures. We used a dominant negative RFP-tagged KASH domain (hereafter KASH) that disrupts LINC complex organization by saturating endogenous SUN domain proteins (73). Rafts generated from lentivirally transduced keratinocytes expressing KASH demonstrate key phenotypic markers of LINC complex disruption, such as an increased nuclear size and an increased distance between the nucleus and the centrosome, which has been shown before (74, 75) (Figure 12 A-D). KASH expression reveals no gross defects in epidermal differentiation (Figure 12A). As indicated above *ITGA6* is significantly positioned toward the nuclear periphery in basal progenitor cells in addition to its polarization (Figure 7 F). To gain mechanistic insight into how the LINC complex influences gene polarization, we compared the peripheral localization of *ITGA6* in RFP and KASH rafts. Intriguingly, we observe only a marginal difference in the radial positioning of the locus (Figure 7G). Analysis of HD gene localization (Figure 13A), however, demonstrates that basal progenitor cells in KASH-expressing raft cultures lose HD gene polarization toward the basement membrane when compared to differentiated suprabasal cells (Figure 13 B). Furthermore, there is a significant difference between the HD gene localizations in the basal progenitor cells of KASH rafts when compared to

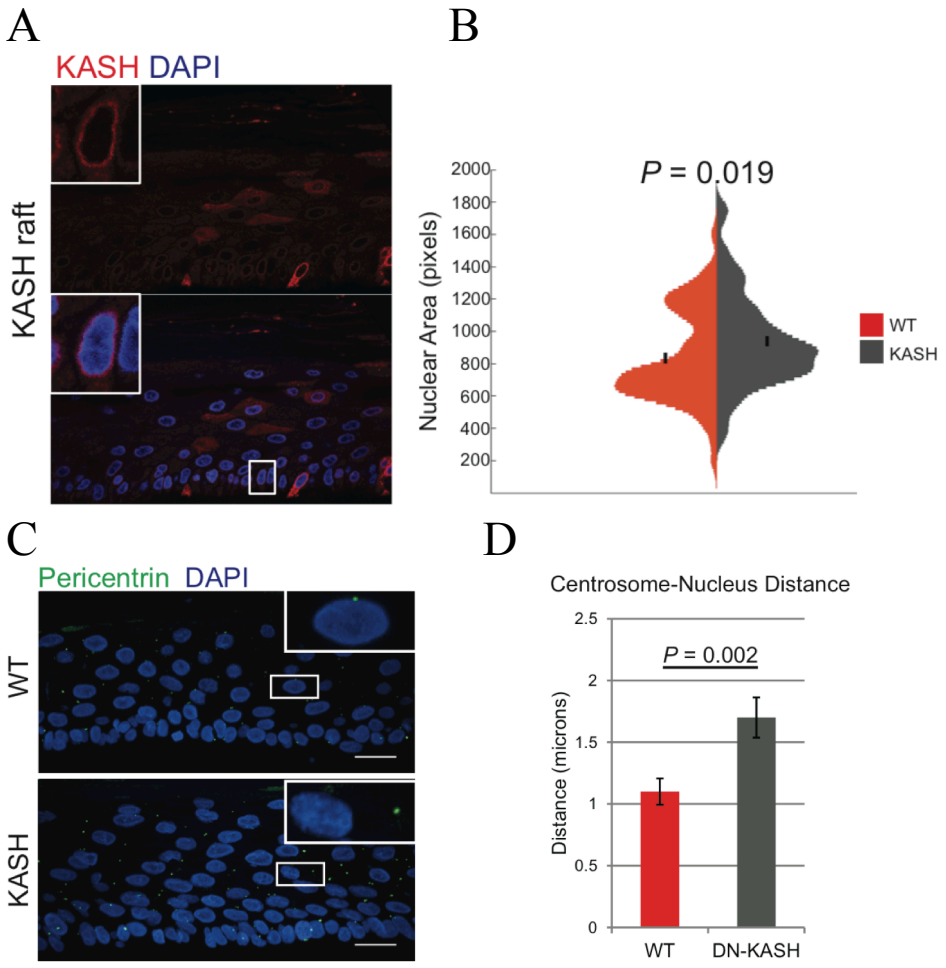

Figure 12: Disruption of the LINC complex causes typical morphological changes in cells

A, Immunofluorescence image showing the localization of KASH (red) at the nuclear perimeter using an antibody targeting RFP in a raft culture derived from KASH-expressing keratinocytes. DAPI (blue) is used as a nuclear counterstain. **B**, Quantification of nuclear area of WT and KASH-disrupted raft cultures. N=80 nuclei for WT and N=88 nuclei for KASH rafts. *P* value derived from two-tailed Student's t-test. **C**, Immunofluorescence image showing the localization of the centrosome marker pericentrin (green) in WT and KASH-expressing raft cultures. DAPI

(Figure 12 cont.)

(blue) is used as a nuclear counterstain. **D**, Quantification of the distance between the centrosome to the closest nuclear edge in WT and KASH-disrupted raft cultures. N=258 cells for WT rafts and N=263 cells for KASH rafts. For all data, error bars represent the standard error of the mean and P values derived from two-tailed Student's t-test. Scale bar is equal to 20 μm for all images.

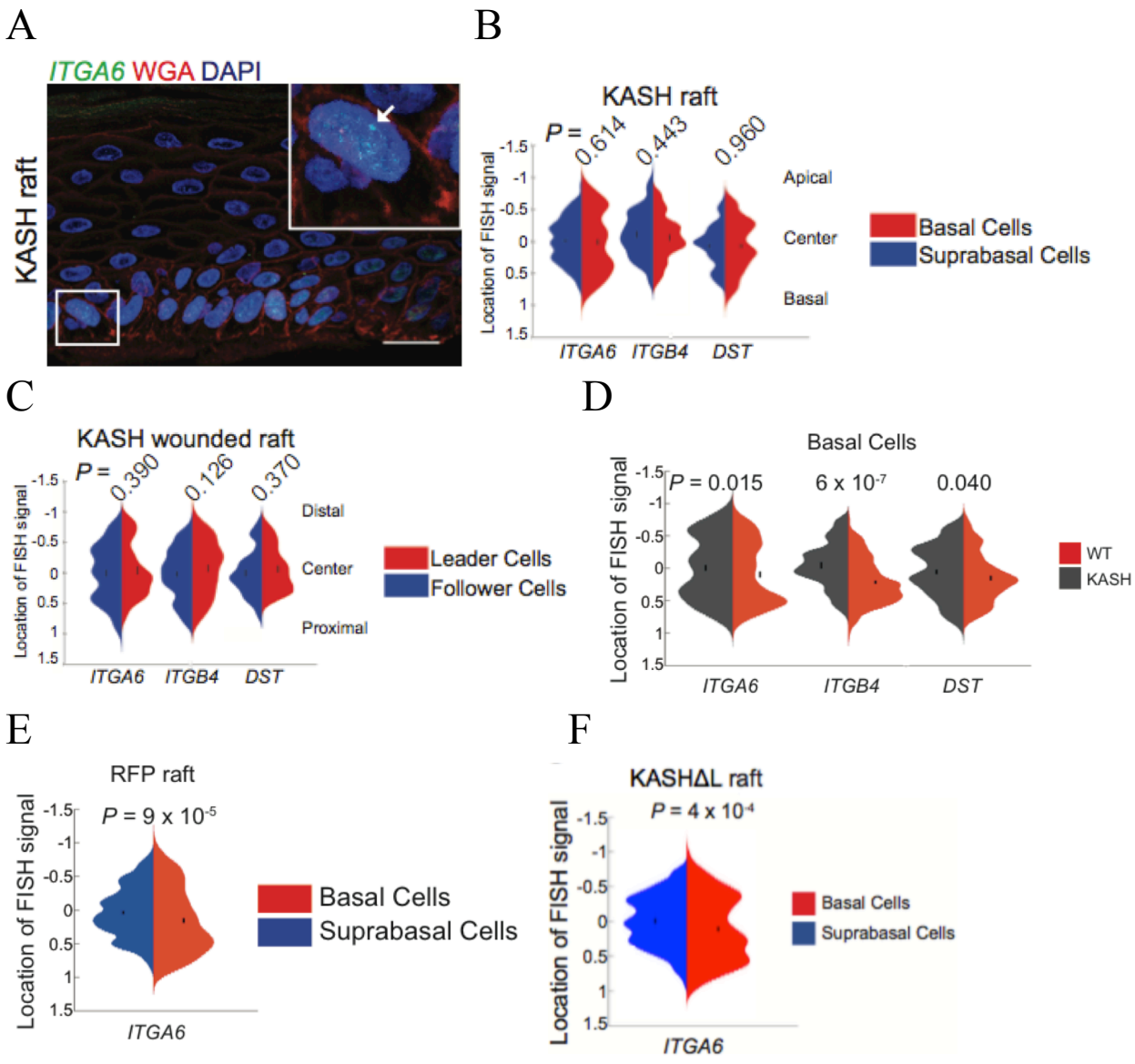

Figure 13: Disruption of the LINC complex causes loss of HD gene polarity

A, FISH image showing an HD gene, *ITGA6* (green), relative to the basement membrane in a raft expressing the dominant negative KASH domain. WGA (red) demarcates cell membranes and DAPI (blue) is used as a nuclear counterstain. Arrow in image insert highlights FISH signal localization. Scale bar is equal to 20 µm. **B**, Normalized gene positions relative to the basement

(Figure 13 cont.)

membrane in basal (red) and suprabasal cells (blue) in KASH-disrupted raft cultures. For *ITGA6*, N = 137 (basal cells) and 274 (suprabasal cells) loci. For *ITGB4*, N = 57 (basal cells) and 58 (suprabasal cells) loci. For DST, N = 148 (basal cells) and 124 (suprabasal cells) loci. **C**, Comparison of HD gene localization relative to the leading edge in leader (red) and follower cells (blue) of wounded KASH disrupted raft cultures. For *ITGA6*, N = 31 (leader cells) and 59 (follower cells) loci. For *ITGB4*, N = 55 (leader cells) and 120 (follower cells) loci. For *DST*, N = 42 (leader cells) and 50 (follower cells) loci.). **D**, Comparison of HD gene positions in basal cells of WT (red) and KASH-expressing (gray) raft cultures. N values and replicates are listed in the legend for Fig 1 and Fig 11. **E**, Comparison of normalized positions of *ITGA6* in basal (red) and suprabasal (blue) cells of RFP expressing raft cultures. N=199 loci for basal cells and N=389 loci for suprabasal cells. **F**, Comparison of normalized positions of *ITGA6* in basal (red) and suprabasal (blue) cells of KASHΔL expressing raft cultures For all quantifications, error bars represent the standard error of the mean and *P* values derived from two-tailed Student's t-test. For (**B**), results are pooled from 3 KASH rafts (biological replicates). For (**C**), results are pooled from 2 wounded KASH rafts (biological replicates). For (**D-F**), data points are pooled and derived from 3 different rafts (biological replicates) per condition.

WT rafts (Figure 13 D). As controls, we generated rafts from lentivirally transduced keratinocytes with an RFP empty vector (hereafter RFP), as well as an RFP-KASH domain lacking the luminal SUN-binding domain (hereafter KASHΔL). Both the basal progenitor cells of RFP-expressing and KASHΔL-expressing rafts maintain *ITGA6* gene polarity and the distribution of the loci significantly differs when compared to that of suprabasal cells (Figure 13 E-F). H&E staining of raft cultures demonstrates that KASH Expressing rafts have a significantly higher degree of separation from their underlying substrate within the tissue when compared to WT and KASHΔL-expressing rafts (Figure 14 A-B). These experiments indicate that the loss of HD gene polarity mediated by KASH overexpression contributes to overall HD dysfunction in the absence of gene polarity.

We then examined the effect perturbing the LINC complex on HD gene polarity in wounded raft cultures. A wound assay in KASH-expressing raft cultures revealed no differences in HD gene localization toward the leading edge in leader cells compared to follower cells (Figure 13C), contrary to what we showed in WT cells (Figure 9C), indicating that the LINC complex is necessary in maintaining HD gene polarity in migrating keratinocytes at the leading edge in wounded raft cultures.

Analysis of HD gene polarity in wild type and Syne2 KO mice

To determine the effect of the LINC complex on gene positioning *in vivo*, we analyzed knockout mice that lack the actin-binding domain of nesprin-2 gene, *Syne*2. Here, we find that *Itgb4*, the mouse homolog of human *ITGB4*, is significantly polarized to the basal side of nuclei in basal

progenitor cells when compared to suprabasal cells in tongue-derived epidermal tissue of wild type (WT) mice (Figure 15 A-B). However, there is no difference in the positioning of *Itgb4* between basal and suprabasal cells in *Syne2* KO mice (Figure 15 A-B). To further highlight this effect, we directly compared only the subnuclear positioning of *Itgb4* in basal cells of the epidermal tissue of WT and *Syne2* KO mice. Here, we find a significant difference between the two populations and find that, importantly, the polarization of *Itgb4* in the basal cells of WT mice is lost when compared to *Syne2* KO mice. (Figure 15C). Together, these results support that the HD-ECM interaction is linked to gene polarization, and the further implicate the LINC complex in mediating this signal.

The effect of the LINC complex on nuclear orientation

It is widely understood that in basal progenitors the centrosome is positioned apically to the nucleus along the longitudinal axis (76). Therefore, we examined whether disruption of the LINC complex affects the centrosome positioning relative to the nucleus by measuring the angle of centrosome to nuclear centroid (Figure 16A). A histogram plot in polar coordinates demonstrates a striking loss of apical polarity in the presence of dominant negative KASH (Figure 16B). This result suggests that the LINC complex is needed to maintain correct orientation of the nucleus to ensure the peripherally localized HD gene loci are adjacent to the basement membrane.

The effect of HD gene polarity on mRNA localization

Loss of HD gene polarity precedes gross impairment of tissue polarity in the detachment assay (Figure 10-11). We hypothesized that gene polarity functions to position mRNA for efficient

A

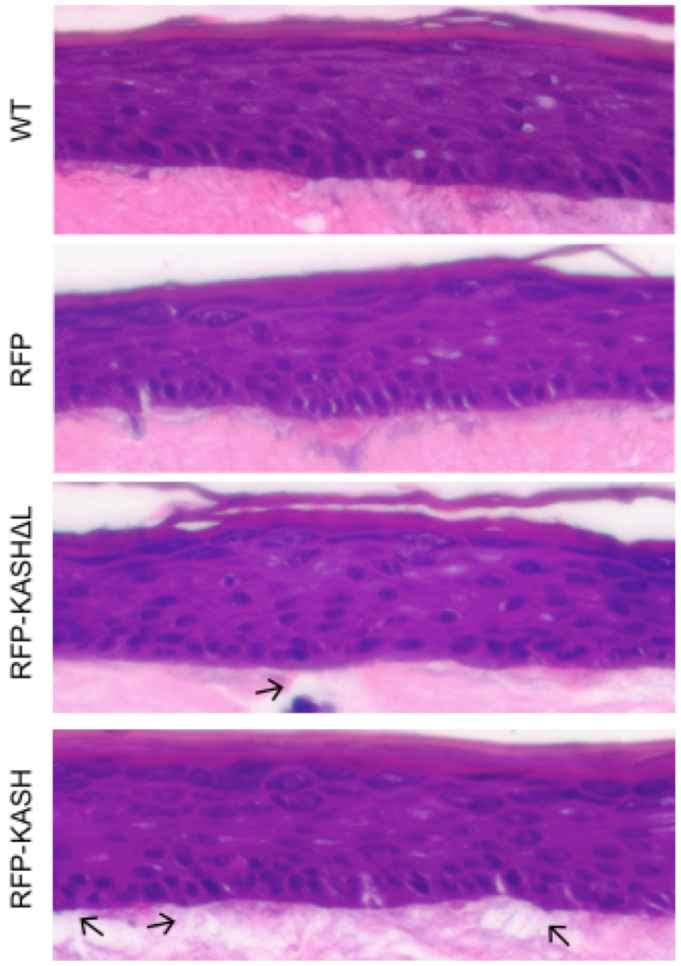
WT
RFP
RFP-KASHΔL
RFP-KASH

B

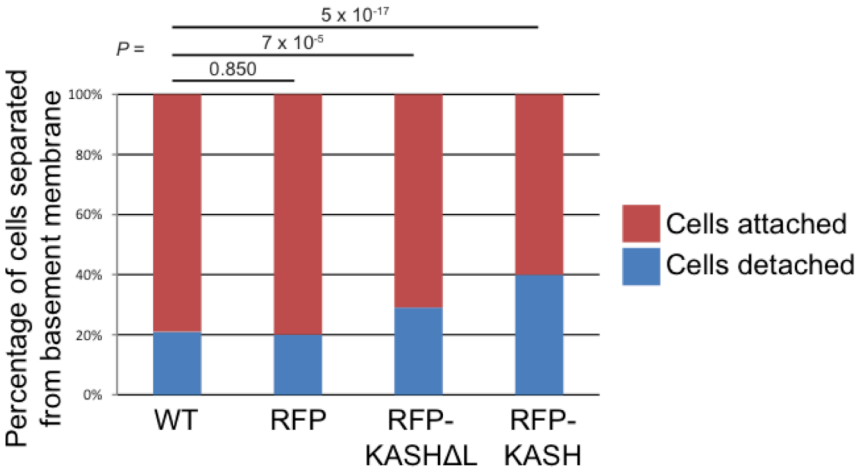
P =
5 x 10-17
7 x 10-5
0.850
Percentage of cells separated from basement membrane
100%
80%
60%
40%
20%
0%
WT
RFP
RFP-KASHΔL
RFP-KASH
Cells attached
Cells detached

Figure 14: Basal progenitor cell detachment in KASH-expressing rafts

A, Representative images of H&E stained raft cultures. Arrows highlight areas of separation between basal cells and the underlying substrate. **B**, Percentage of basal cells that remain attached (red) compared to cells that have separated (blue) from their underlying substrate. Total cells analyzed (N) are as follows: 799 (WT), 944 (RFP), 894 (RFP-KASHΔL), and 886 (RFP-KASH). Each condition represents pooled results from 2 rafts. *P* values derived from chi-squared test.

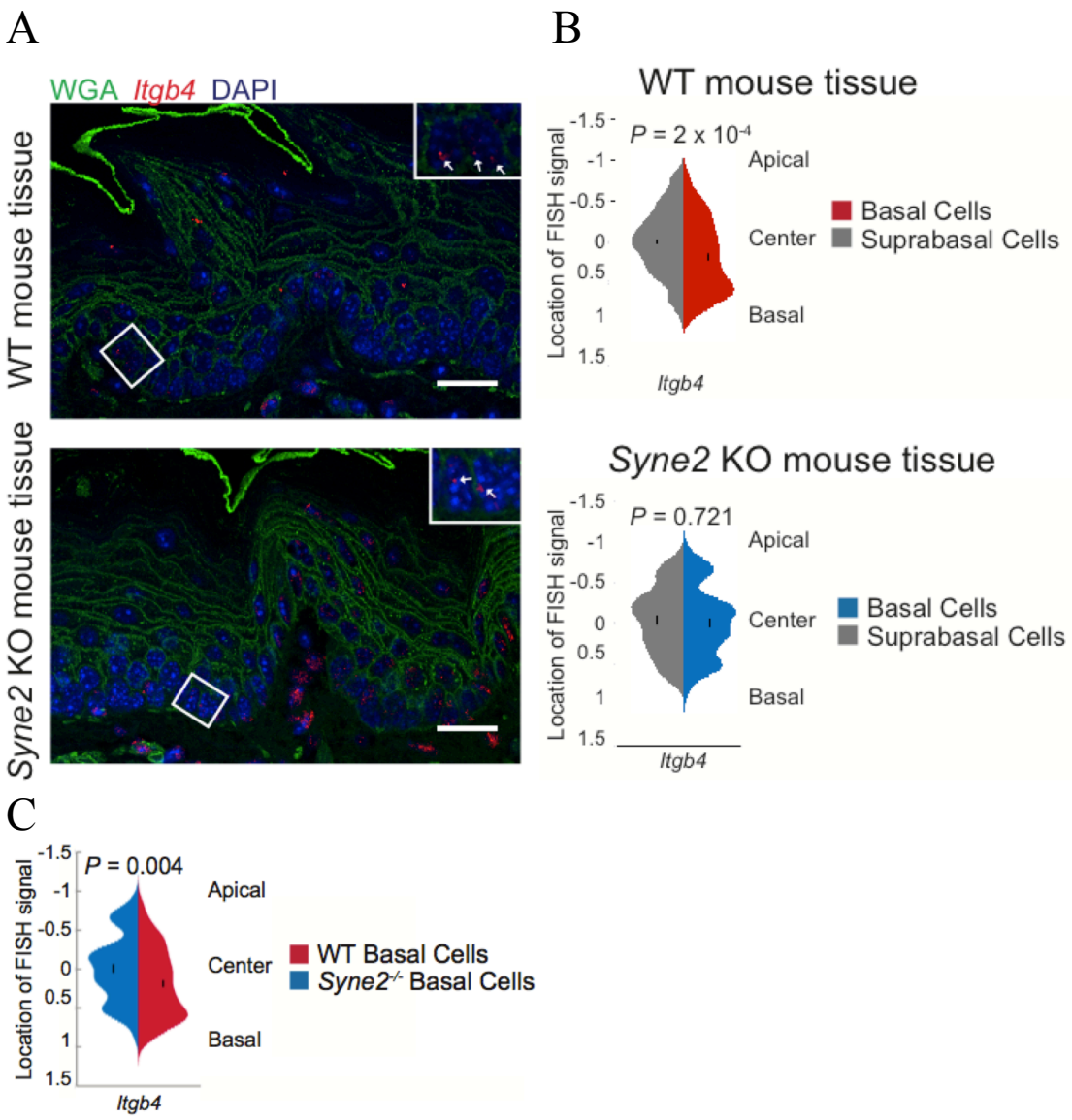

Figure 15: HD genes are polarized in the mouse epidermis

A, ImmunoFISH showing the position of *Itgb4* (red) in mouse epidermal tissue. WGA (green) demarcates cell membranes and DAPI (blue) is used as a nuclear counterstain. Scale bar is equal to 20 µm. **B,** Normalized gene position of *Itgb4* in basal and suprabasal cells of WT mouse tissue (N = 117 loci for basal cells and N = 160 loci for suprabasal cells) and *Syne2* KO mouse tissue (N = 61 loci for basal cells and N = 51 loci for suprabasal cells). **C**, Comparison of the normalized gene position of *Itgb4* between the basal cells of WT and *Syne2* KO mouse tissue.

(Figure 15 cont.)

For N values, see legend for Fig. 3B. For all quantifications, error bars represent the standard error of the mean and *P* values derived from two-tailed Student's t-test.

translation toward the side of the cell relevant to its encoded protein's function. Since detachment of the raft results in overall RNA disorder (data not shown), we chose to examine mRNA polarization in the context of LINC complex perturbation. The dominant negative phenotype of the KASH domain does not lead to a loss of epidermal morphology; thus, it is a milder effect that allows us to uncouple mRNA distribution from tissue organization. In order to visualize and quantify mRNA in individual cells, we performed single molecule mRNA FISH (smFISH) using probe sets consisting of 30-50 singly labeled 20mer DNA oligomers targeting tandem regions of exons (77). This hybridization reveals diffraction limited spots in individual cells, which represent single mRNA particles that can be quantified based on their intensity profiles. The *ITGB4* locus probe set provided the highest signal to noise ratio in tissue thin sections, and it was therefore chosen to test whether HD mRNAs are polarized in the genetically polarized basal cells of raft cultures. Our automated analysis demonstrates that *ITGB4* mRNA particles are indeed polarized to the basal side of the cell where their protein products are localized and that this mRNA polarity is lost in KASH overexpressing rafts (Figure 17 A-B). Intriguingly, we also detect that loss of mRNA polarization coincides with a significant increase of total mRNA particles per cell in KASH-expressing rafts when compared to WT rafts (Figure 17C). Quantitative PCR analysis confirms transcriptional misregulation of HD expression when the LINC complex is disrupted, while our control gene *KRT14*, a genes that encodes an intermediate filament specific to the basal cells of the epidermis, shows no difference in RNA levels (Figure 17D).

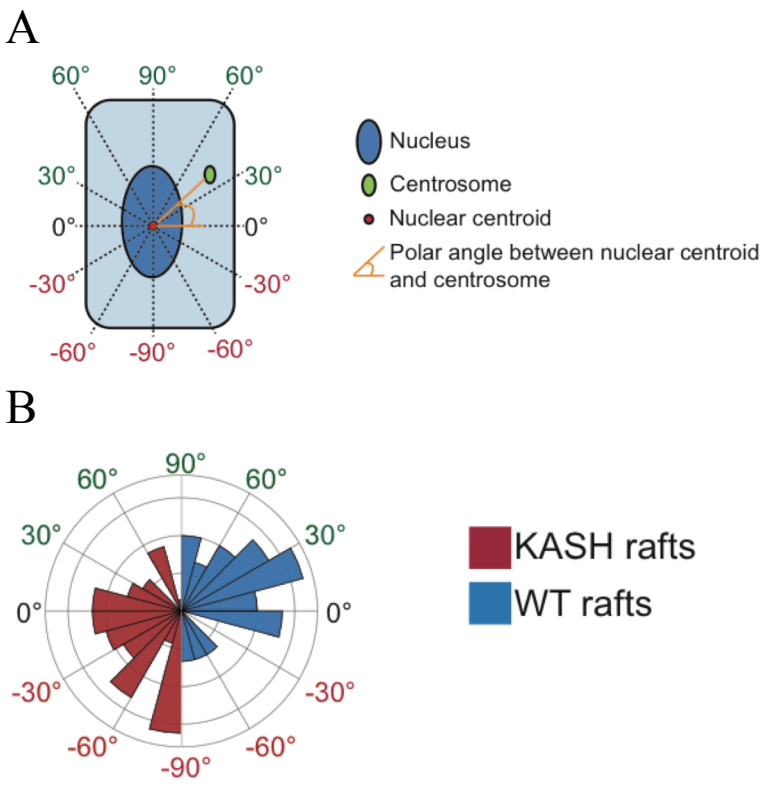

Figure 16: Disruption of the LINC complex causes a mislocalization of centrosome position in basal cells of raft cultures

A, Schematic for measuring polar angle of the centrosome relative to the nuclear centroid. The reference (0^o) is chosen as the line parallel to the basement membrane that intersects the nuclear centroid. Positive angles (green) represent apical positions of the centrosome, while negative angles (red) represent basal positions. **B**, Radial histogram depicting the localization of the centrosome relative to the nuclear centroid in KASH (left, red) and WT (right, blue) rafts.

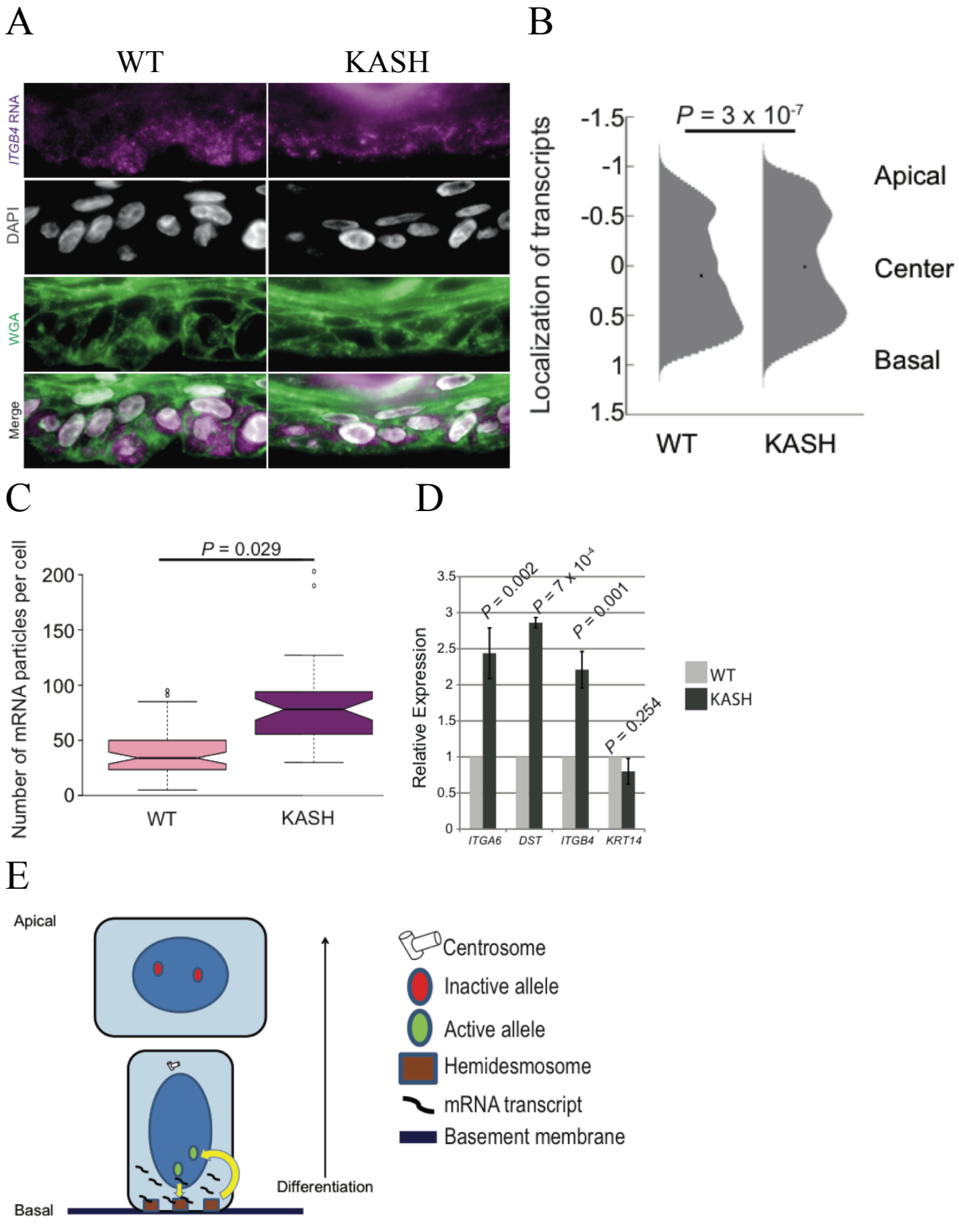
A
WT
KASH
ITGB4 RNA
DAPI
WGA
Merge
B
P = 3 x 10-7
Localization of transcripts
-1.5
-1
-0.5
0
0.5
1
1.5
Apical
Center
Basal
WT
KASH
C
P = 0.029
Number of mRNA particles per cell
200
150
100
50
0
WT
KASH
D
P = 0.002
P = 7 x 10-4
P = 0.001
P = 0.254
Relative Expression
3.5
3
2.5
2
1.5
1
0.5
0
ITGA6
DST
ITGB4
KRT14
WT
KASH
E
Apical
Basal
Differentiation
Centrosome
Inactive allele
Active allele
Hemidesmosome
mRNA transcript
Basement membrane

Figure 17: Nuclear polarity of the *ITGB4* locus correlates with cellular polarization of its mRNA and transcriptional regulation

A, RNA FISH image demonstrating *ITGB4* single mRNA particles (magenta) in both WT and KASH-disrupted raft cultures. DAPI (gray) is used as a nuclear counterstain and WGA (green) is used to demarcate cell membranes. Scale bar = 20 μm. **B**, Normalized positions of individual *ITGB4* mRNA particles relative to the basement membrane in WT and KASH-disrupted raft cultures. For WT rafts, N = 2230 mRNA particles pooled from 61 different cells. For KASH rafts, N = 2983 mRNA particles pooled from 40 different cells. Bars represent standard error of the mean and *P* value is derived from a two-tailed Student's t-test. **C**, Quantification of the number of *ITGB4* mRNA particles per cell measured by smFISH in WT and KASH-disrupted raft cultures. N = 61 cells for WT rafts and N = 40 cells for KASH rafts. *P* value is derived from a two-tailed Student's t-test. For box plots, center lines show the medians, box limits indicate 25^{th} and 75^{th} percentiles, whiskers extend 1.5 times the interquartile range from the 25^{th} and 75^{th} percentiles, and outliers are represented by dots. **D,** Relative expression by qPCR of various HD genes in WT and KASH-disrupted raft cultures. Expression levels represent the average of 3 replicates. Bars represent the standard deviation and *P* values are derived from a two-tailed Student's t-test. **E**, Model of the functional relationship among HD gene, mRNA, and protein polarization in basal progenitor keratinocytes. Polarization of HD gene loci informs the distribution of their encoded mRNAs, but is in turn informed by the subsequent polarized communication of HD complexes and their interaction with the ECM at the basal cell interface.

CHAPTER IV

Discussion

Potential mechanisms driving HD gene polarity

It has been proposed that changes in genome organization during cellular differentiation are dependent on mitosis (78). This is partly due to the dense nuclear environment during interphase, which leads to restricted chromatin movement (79). Chromatin decondensation during cell division provides an opportunity for the genome to re-organize during early G1 phase (80). This genome re-shuffling can be driven through the association of architectural proteins with DNA, which can drive the localization of DNA sequences through the binding of certain nuclear landmarks upon nuclear reformation (81).

In contrast to the proposed "static" nature of the genome during interphase, it has been observed that certain stimuli can cause the dynamic movement of chromatin during interphase. For example, Hsp70 transgenes have been shown to dynamically move to associate with nuclear speckles following heat shock to facilitate increased levels of transcriptional activation (82). Furthermore, cell cycle-independent movement of chromosome territories (CTs) have been observed after the introduction of cellular stresses such as serum starvation and DNA damage (83, 84). In these cases, it is suggested that an active process involving nuclear actin filaments and nuclear myosin motors mediates this dynamic chromatin movement (82, 84, 85). Nuclear F-actin has previously been proposed to be involved in the nuclear movement of certain DNA sequences, such as the movement of U2 gene arrays to Cajal bodies or upon movement of a gene

array from the periphery to the interior of the nucleus upon targeting of a transcriptional activator (86, 87). This concept of an active mechanism driving chromatin movements or genome re-organization is in contrast to the proposed mechanism of genome re-organization requiring mitosis, which potentially requires the dissolution of the nuclear envelope so that chromatin can reorganize upon the re-assembly of the nucleus. This has been proposed to be mediated by various processes, such as through a mechanism of differential binding of LADs to the nuclear lamina upon nuclear envelope re-emergence or through concerted chromosome association driven through coordinate gene regulation (88, 89). Nonetheless, in the context of epithelial cell migration, it is unlikely that cells at the leading edge undergo proliferation during the period of migration (90); therefore, gene polarity induced by migration during epidermal wound healing in raft cultures (Figure 9) must likely involve a separate process.

It has been shown that in certain models of polarized cell migration, cells at the leading edge triggers the rotation of their nuclei during the initial nuclear re-positioning after induction, so that its long axis is oriented perpendicular to the leading edge (91-93). Interestingly, it is suggested that the LINC complex is required for nuclear rotation during cell migration (93). We have shown that in KASH-expressing wounded raft cultures, there is a marked loss of polarized HD gene positioning towards the leading edge when compared to WT wounded rafts (Figure 9C and 13C). Here, HD gene loci may not be actively moved towards the leading edge, but rather be dependent on LINC complex-mediated nuclear rotation to "passively" position the loci as a function of a global coordinated process. In this scenario, the cell must be able to differentiate the side of the nucleus that HD genes are more likely to reside in. Further research, however, is needed to identify the precise mechanisms of HD gene polarity in epidermal wound healing.

Furthermore, when migrating epidermal cells contact other cells at the opposite edge of the wound, leader cells lose front/rear polarity. It would be interesting to examine whether HD genes lose polarity with respect to the leading edge of the cell or if they remain in their positions upon wound closure.

We also show that there is a loss of the apical centrosome positioning in KASH rafts (Figure 16), which has been implicated in processes ranging from cell migration to epithelial-to-mesenchymal transition (94, 95). The loss of apical centrosome positioning suggests that disrupting the LINC complex impacts nuclear orientation in basal progenitor cells (94, 95). In support of this, nuclei within cells have been shown to continuously spin in the absence of lamin B1, indicating that the LINC complex may play a role in keeping the nucleus fixed within the cellular space (96). Therefore, in basal progenitor cells, the LINC complex may function to "lock-in" the native genomic organization to specifically position HD genes for regulatory synergy with the ECM. However, how this native genomic organization manifests itself initially still remains to be understood. It is important to note that basal progenitor cells are the only mitotically active cells of the epidermis. Therefore, the emergence of chromosomal topologies that facilitate HD gene positioning towards the basal side of the nucleus may be a function of global changes in genome organization that occur through a round of cell division. Mitosis-dependent changes in genome organization have been observed in other models of differentiation, such as during myogenesis (97). However, an active mechanism at the local level, such through nuclear F-actin and molecular motors as described previously, must not be ruled out as a potential mechanism for HD gene polarity. If an active mechanism is required for nuclear movement of HD alleles, it would be interesting to note whether this transport simply

positions the loci at the basal side of the nucleus, or directs them to a nuclear landmark such as a subnuclear body for gene regulation.

HD genes within the nuclear microenvironment

The position of a gene locus within nuclear space can affect its ability to be transcribed. Factors that can influence a gene's transcriptional ability are its location relative to its CT or its radial position relative to the periphery of the nucleus. Active genes tend to be localized at the periphery of their CTs where a higher concentration of transcription machinery may reside in the interchromosomal space (98). Alleles buried within their CTs may be devoid of transcription machinery due to volume exclusion in a crowded environment. An allele can also become looped away from its CT to associate with a transcription factory to allow for robust gene expression (2). We show that *ITGA6* is positioned more towards the basal side of its CT, HSA2, in basal cells when compared to suprabasal cells in raft cultures (Figure 7C). This basal localization could partly explain the tendency of the gene to be more polarized towards the basement membrane in basal progenitor cells. Furthermore, on the whole, *ITGA6* is positioned more towards the periphery of HSA2 in basal cells, while the gene moves internal upon differentiation (Figure 7C). This spatial regulation could partly explain the loss of *ITGA6* expression upon differentiation.

Gene positioning relative to the nuclear periphery is an important factor in the regulation of gene expression. The nuclear periphery, characterized by the presence of the nuclear lamina and its association with heterochromatin, tends to be a largely transcriptionally repressive environment (99). Intriguingly, we show that *ITGA6* loci tend to be more peripherally localized within the

nucleus in basal progenitor cells when compared to differentiated suprabasal cells (Figure 7F). This trend is in contrast to the expected position of these genes, as active genes are usually more centrally localized than transcriptionally silent genes. However, the peripheral localization of the *ITGA6* locus could be a byproduct of its basal localization, as a gene that is more polarized towards the basement membrane will be more likely to be closer to the nuclear membrane as a result. This suggests that polarity within the nucleus could be considered a new mechanism of nuclear organization in regulating gene expression.

Crosstalk between HD gene and protein polarity

We show during a time course that HD gene polarity and protein polarity is lost upon detachment of raft cultures from their underlying substrate (Figure 10 and 11). The loss of gene polarity as early as 2 hours and protein polarity at 8 hours after raft detachment (Figure 10 and 11), suggests that the former is upstream of the latter and that detachment leads to a loss of communication between the nucleus and the HD protein complex. This implies that upon detachment, or loss of the integrin-ECM connection, there is a mechanical signal to the nucleus that induces the loss of gene polarization, and this loss of gene polarization then leads to the loss of protein polarity. We suggest that the cause of the loss of gene polarity is mediated through the LINC complex, however how the mechanism by which LINC complex does so remains to be understood.

We suggest that gene polarization functions to pre-position mRNAs towards their sites of active translation to facilitate efficient incorporation of HD components to the basal side of progenitor cells in raft cultures (Figure 17A-B). In the event of attenuated gene polarization post-raft detachment, this potential loss of transcript localization could explain the loss of protein

polarization at the basal side of progenitor cells. It would be interesting to see whether transcription of HD genes is affected post-detachment in K10-negative cells.

Subnuclear gene positioning and expression

While mRNA polarization has been previously observed in the context of targeting sequences, such as with *ACTB* mRNA particles to sites of actin polymerization and remodeling at lammellopodia in migrating cells or at dendritic spines in neurons (100, 101), these types of localization events have not been related to nuclear organization.

It has been shown that after transcription, transcripts move through the nucleus through random diffusion until they are able to associate with a nuclear pore prior to nuclear export (102). We propose that gene polarity allows for a higher probability that HD mRNAs will localize and export at the basal side of the nucleus due to the initial proximity of the transcription site. In other words, the direction towards basal nuclear export could represent the "path of least resistance" in a crowded nuclear space. We show that *ITGB4* mRNA has a propensity to be localized to the basal side of basal progenitor cells, but this localization is not exclusive as the transcript is also detected apically (Figure 17 A-B). This could be explained if the *ITGB4* mRNA travels randomly throughout the nucleus before export, as although we predict most will export through nearer nuclear pores at the basal side of the nucleus, a smaller percentage of *ITGB4* mRNA particles may travel through the nuclear volume before contacting a nuclear pore at the apical nuclear edge. Furthermore, it has been proposed that the crowded nuclear environment prevents mRNA particles from travelling in a random walk given the physical constraints imposed by chromatin. Instead, mRNA may move by Brownian movement in defined

channels in the interchromosomal space; however, these channels serve as pathways to direct mRNA travel in defined one-dimensional direction of diffusion to nuclear pores (103). In this scenario, *ITGB4* mRNA could be limited to export at basal nuclear pores given a defined channeled pathway.

Given the bifurcation of basal progenitor cells of the epidermis caused by their apical/basal polarity, it is possible that the apical side of the cells contains no or fewer transport machinery to direct HD mRNA to the basal side of the cells. Like in the nucleus, mRNPs in the cytoplasm, when not being actively targeted for localization, move via simple diffusion (104); therefore, if transport machinery specific to *ITGB4* mRNA predominantly localized to the basal side of the cell, then the *ITGB4* messenger ribonucleoprotein complexes (mRNPs) are more likely to be detected and transported if they are diffusing in the basal side of the cells. Furthermore, it is possible that *ITGB4* mRNPs are not targeted by transport proteins, and instead are preferentially positioned at the basal side of the cells as a result of preferential positioning in the nucleus and movement by Brownian motion. Furthermore, there may be a diffusion barrier that exists once the mRNP has exported into the cytoplasm to prevent the transcripts from being mislocalized. It remains to be determined whether *ITGB4* transcripts are positioned by an active or passive process, and whether there contain any targeting "zip code" sequences within the gene.

We have previously shown that bi-allelic proximity in single nuclei attenuates variability in gene expression (97) (Figure 18). Disruption of the LINC complex causes a loss of gene polarity as well as an increase in HD gene expression (Figure 17 C-D). This suggests that the LINC complex may buffer the levels of HD transcription to prevent an over abundance of transcripts.

This buffer could serve to prevent excess HD proteins, which may incorporate into non-basal areas of the plasma membrane. It would be interesting to see whether the LINC complex reduces HD transcriptional noise as a means to regulate epidermal differentiation. Furthermore, we have not taken into account the transcriptional activity of individual alleles when accounting for gene polarity. As even "active" genes are not universally "on" due to transcriptional bursting (105), it would be interesting to examine whether transcriptionally active HD alleles are more likely to be polarized than transcriptionally inactive alleles at any given time.

Concluding Remarks

Asymmetric protein distribution is critical in cell function, differentiation, and disease (106, 107). Whether the many examples of nonrandom nuclear organization may also include the localization of genes relative to their protein products in the cell has gone largely unexplored3. Differentiation is often accompanied by changes in the spatial organization of the genome (108, 109), which is evident during mouse epidermal differentiation (110). Here, we demonstrate that core HD genes are polarized to the side of the nucleus where their protein products are functionally localized in the basal layer of progenitor keratinocytes of organotypic epidermal raft cultures and toward the leading edge of nuclei in leader cells during wound healing. Moreover, we find that perturbation of the epithelium by loss of contact to the ECM or manipulation of the LINC complex results in the loss of gene polarization. The standard view of gene positioning at the periphery has been its role as a repressive nuclear compartment (26, 111). Intriguingly, in the case of HD gene polarization, the localization of genes toward the basal side of the nucleus appears to attenuate their expression. Thus, polarization of HD gene loci informs the distribution of their encoded mRNAs and proteins, but is in turn informed by the subsequent polarized

communication of HD complexes through their interaction with the ECM (Figure 17E). Nonetheless, the loss of apical positioning of the centrosome in KASH rafts (Figure 16) suggests that disrupting the LINC complex impacts nuclear orientation, which may serve to "lock-in" the native genomic organization of basal progenitors and, as a function, HD gene polarity. We suggest that 'genetic polarization' represents a new mode of gene regulation, such that genes are positioned within the nucleus to facilitate the functional distribution of their encoded proteins, and may likely be of broad importance in establishing other forms of cellular and tissue asymmetry.

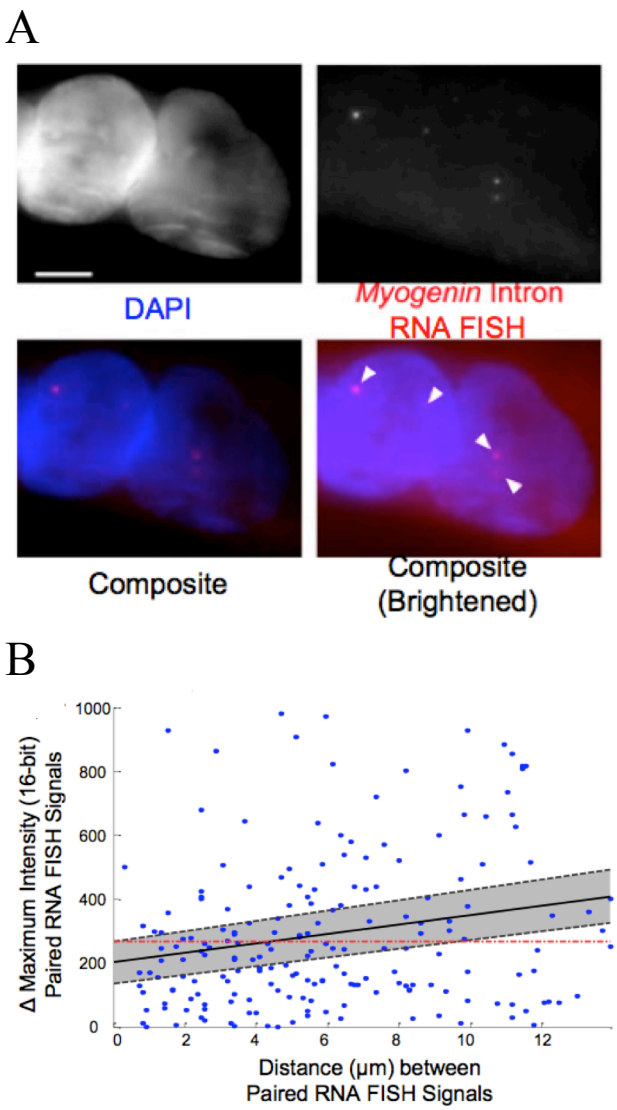

Figure 18: Spatial proximity of *myogenin* alleles influences bi-allelic transcriptional variability in myotubes

A, RNA FISH image showing the subnuclear position of *MYOG* active transcription sites in MyoD expressing myotubes. *MYOG* intronic RNA FISH signal is shown in red and DAPI is shown in blue. Scale bar equals 5 μm **B**, Scatterplot showing the difference in intensity between two *MYOG* intronic RNA FISH signals in single cells as a function of distance in microns. Gray

(Figure 18 cont.)

area represents 95% confidence interval and the solid line represents the best fitting line. Red dashed line represents the expected fit of a line with a slope of zero. 0.2174 ± 0.1196, Pearson Correlation. *P* value = 0.0021. N = 194 nuclei. Figure adapted from Neems et al. (97).

Table 1: N-values for Figure 9

Gene	K10 Positive/Negative	Time Course	N value (number of loci)
ITGA6	Negative	15 min	50
ITGA6	Positive	15 min	91
ITGA6	Negative	2 hr	52
ITGA6	Positive	2 hr	107
ITGA6	Negative	8 hr	59
ITGA6	Positive	8 hr	144
ITGA6	Negative	16 hr	60
ITGA6	Positive	16 hr	140
ITGA6	Negative	24 hr	67
ITGA6	Positive	24 hr	82
ITGB4	Negative	15 min	96
ITGB4	Positive	15 min	73
ITGB4	Negative	2 hr	86
ITGB4	Positive	2 hr	88
ITGB4	Negative	8 hr	48
ITGB4	Positive	8 hr	58
ITGB4	Negative	16 hr	49
ITGB4	Positive	16 hr	41
ITGB4	Negative	24 hr	48
ITGB4	Positive	24 hr	86
DST	Negative	15 min	204
DST	Positive	15 min	202
DST	Negative	2 hr	81
DST	Positive	2 hr	76
DST	Negative	8 hr	68
DST	Positive	8 hr	91
DST	Negative	16 hr	54
DST	Positive	16 hr	64
DST	Negative	24 hr	71
DST	Positive	24 hr	43

Table 2: List of BACs used in this study.

Gene	BAC ID	Chromosome	Species
ITGA6	RP11-227L6	2	Human
ITGB4	RP11-749C2	17	Human
DST	RP1-61B2	6	Human
GAPDH	RP11-369N23	12	Human
DSP	RP11-177C16	6	Human
Itgb4	RP23-280P15	11	Mouse

Table 3: RNA FISH probe sequences for *ITGB4*.

Probe sequence (5' to 3')	Probe name
agaggctgacgctgatcaag	ITGB4 exons_1
ttatccacacggacacactc	ITGB4 exons_2
gtggtgtcaatctgggtctc	ITGB4 exons_3
ctcaaaatgccgctcctcac	ITGB4 exons_4
atggagttggagaagtccat	ITGB4 exons_5
ttgaggttgtccagatcatc	ITGB4 exons_6
aatagtgtagtcgctggtga	ITGB4 exons_7
tttgtccacaaacttgccaa	ITGB4 exons_8
gttcttgaaggagaaggggg	ITGB4 exons_9
tctgcaggatggcatcgaag	ITGB4 exons_10
catcagcctcatagtggaag	ITGB4 exons_11
catcgttgcggctcatgatg	ITGB4 exons_12
tggtgacagcaaagatgggg	ITGB4 exons_13
ctcgtagtagctataggagt	ITGB4 exons_14
ttctggaacatcttggaggt	ITGB4 exons_15
cagctgcacctggtatatac	ITGB4 exons_16
aggtttcagatggatgttgc	ITGB4 exons_17
atcttgaggccgtcggagaa	ITGB4 exons_18
cacactgtccgcacacgaag	ITGB4 exons_19
tgaatgtcactcagagagcc	ITGB4 exons_20
gttgtcatactcgcagaact	ITGB4 exons_21
attgcagaggaacccggaag	ITGB4 exons_22
attgctgaggggacagtcac	ITGB4 exons_23
cattgctgtcgatgcaggtg	ITGB4 exons_24
gagtagttgatctcgcagat	ITGB4 exons_25
ttgaagttgcattcctcaca	ITGB4 exons_26
taagctcgtccaccatcttg	ITGB4 exons_27
ctgtaggtgcagtcgtcatc	ITGB4 exons_28
ttcttcttgtgcaccaggac	ITGB4 exons_29
gttgcagcacgggagaagtg	ITGB4 exons_30
catgtagtggtcttccttaa	ITGB4 exons_31
aagtggtcagaggccatcag	ITGB4 exons_32
tgcatgttgttggtgacctt	ITGB4 exons_33
tggcggcatgagtggcaaag	ITGB4 exons_34
agcaggttctcggtgcaaag	ITGB4 exons_35

Table 4: RNA FISH probe sequences for *MYOG*.

Probe sequence (5' to 3')	Probe name
acaggaggtcagctggatag	MYOG introns_1
tcttgtctggaaagaacaca	MYOG introns_2
ggattaatcctcaccctcac	MYOG introns_3
cttttaggctctgactcagg	MYOG introns_4
agtcttctctggtgaacttg	MYOG introns_5
tgggttttctctctgctcag	MYOG introns_6
ctggagttccaatgagactg	MYOG introns_7
atggagacagattttgtggc	MYOG introns_8
ctcctgactctggcgataag	MYOG introns_9
acaggacaccagcttaaagg	MYOG introns_10
atctttgtaactagctcctc	MYOG introns_11
agtgggcagaagtacctgtg	MYOG introns_12
ttctttgatgtctctctctg	MYOG introns_13
taccagtcaggccttactta	MYOG introns_14
gagggactgagggattggag	MYOG introns_15
accggagcaaggaataaggt	MYOG introns_16
ctagagagacccaagggaag	MYOG introns_17
tttgctggtcaagactgcag	MYOG introns_18
ctgcaggagctactatcact	MYOG introns_19
aaggtcaaccaccaggcatc	MYOG introns_20
cagggacattgtcctctctg	MYOG introns_21
actgactcagcacttcacag	MYOG introns_22
aagttggagcaggatggagc	MYOG introns_23
tagggtttggaagcagccac	MYOG introns_24
ttttctgaactcccctagta	MYOG introns_25
acaaagctccggagttctac	MYOG introns_26
ggttttccaggacagatgaa	MYOG introns_27
aatagaggatgggacccttg	MYOG introns_28
tgtaaggggaggtgggaagg	MYOG introns_29

Table 5: Primers used for qPCR analysis

Gene	Forward Primer	Reverse Primer
DST	GAGGCTGGAAGAGGAGGAGATTA	CACTGTTGCCTTCTGACGCT
GAPDH	CCCGCTTCGCTCTCTGCTCCT	CGACCAAATCCGTTGACTCCGAC
ITGA6	ATAACGATGCTGACCCCACG	GCCCAAAGATGTCTCGGGAT
ITGB4	CTGCACAGACGAGATGTTCA	AGGGTGGTGTCAATCTGGGT
KRT14	GCAGTCATCCAGAGATGTGAC	GCCTCAGTTCTTGGTGCGA

References

1. **Cremer T, Cremer C, Baumann H, Luedtke EK, Sperling K, Teuber V, Zorn C. Rabl's model of the interphase chromosome arrangement tested in Chinese hamster cells by premature chromosome condensation and laser-UV-microbeam experiments. Hum Genet. 1982;60(1):46-56.**

2. **Cremer T, Cremer M. Chromosome territories. Cold Spring Harb Perspect Biol. 2010;2(3):a003889.**

3. **Bolzer A, Kreth G, Solovei I, Koehler D, Saracoglu K, Fauth C, Muller S, Eils R, Cremer C, Speicher MR, Cremer T. Three-dimensional maps of all chromosomes in human male fibroblast nuclei and prometaphase rosettes. PLoS Biol. 2005;3(5):e157.**

4. **Boyle S, Gilchrist S, Bridger JM, Mahy NL, Ellis JA, Bickmore WA. The spatial organization of human chromosomes within the nuclei of normal and emerin-mutant cells. Hum Mol Genet. 2001;10(3):211-9.**

5. **Cremer M, von Hase J, Volm T, Brero A, Kreth G, Walter J, Fischer C, Solovei I, Cremer C, Cremer T. Non-random radial higher-order chromatin arrangements in nuclei of diploid human cells. Chromosome Res. 2001;9(7):541-67.**

6. **Tanabe H, Muller S, Neusser M, von Hase J, Calcagno E, Cremer M, Solovei I, Cremer C, Cremer T. Evolutionary conservation of chromosome territory arrangements in cell nuclei from higher primates. Proc Natl Acad Sci U S A. 2002;99(7):4424-9.**

7. **Parada LA, McQueen PG, Misteli T. Tissue-specific spatial organization of genomes. Genome Biol. 2004;5(7):R44.**

8. **Kosak ST, Scalzo D, Alworth SV, Li F, Palmer S, Enver T, Lee JS, Groudine M. Coordinate gene regulation during hematopoiesis is related to genomic organization. PLoS Biol. 2007;5(11):e309.**

9. **Solovei I, Kreysing M, Lanctot C, Kosem S, Peichl L, Cremer T, Guck J, Joffe B. Nuclear architecture of rod photoreceptor cells adapts to vision in mammalian evolution. Cell. 2009;137(2):356-68.**

10. Clowney EJ, LeGros MA, Mosley CP, Clowney FG, Markenskoff-Papadimitriou EC, Myllys M, Barnea G, Larabell CA, Lomvardas S. Nuclear aggregation of olfactory receptor genes governs their monogenic expression. Cell. 2012;151(4):724-37.

11. Solovei I, Wang AS, Thanisch K, Schmidt CS, Krebs S, Zwerger M, Cohen TV, Devys D, Foisner R, Peichl L, Herrmann H, Blum H, Engelkamp D, Stewart CL, Leonhardt H, Joffe B. LBR and lamin A/C sequentially tether peripheral heterochromatin and inversely regulate differentiation. Cell. 2013;152(3):584-98.

12. Noordermeer D, de Laat W. Joining the loops: beta-globin gene regulation. IUBMB Life. 2008;60(12):824-33.

13. Lomvardas S, Barnea G, Pisapia DJ, Mendelsohn M, Kirkland J, Axel R. Interchromosomal interactions and olfactory receptor choice. Cell. 2006;126(2):403-13.

14. Rouquette J, Genoud C, Vazquez-Nin GH, Kraus B, Cremer T, Fakan S. Revealing the high-resolution three-dimensional network of chromatin and interchromatin space: a novel electron-microscopic approach to reconstructing nuclear architecture. Chromosome Res. 2009;17(6):801-10.

15. Cremer T, Cremer C. Chromosome territories, nuclear architecture and gene regulation in mammalian cells. Nat Rev Genet. 2001;2(4):292-301.

16. Volpi EV, Chevret E, Jones T, Vatcheva R, Williamson J, Beck S, Campbell RD, Goldsworthy M, Powis SH, Ragoussis J, Trowsdale J, Sheer D. Large-scale chromatin organization of the major histocompatibility complex and other regions of human chromosome 6 and its response to interferon in interphase nuclei. J Cell Sci. 2000;113 (Pt 9):1565-76.

17. Branco MR, Pombo A. Intermingling of chromosome territories in interphase suggests role in translocations and transcription-dependent associations. PLoS Biol. 2006;4(5):e138.

18. Morey C, Kress C, Bickmore WA. Lack of bystander activation shows that localization exterior to chromosome territories is not sufficient to up-regulate gene expression. Genome Res. 2009;19(7):1184-94.

19. **Verschure PJ, van der Kraan I, Manders EM, Hoogstraten D, Houtsmuller AB, van Driel R. Condensed chromatin domains in the mammalian nucleus are accessible to large macromolecules. EMBO Rep. 2003;4(9):861-6.**

20. **Ferrai C, Xie SQ, Luraghi P, Munari D, Ramirez F, Branco MR, Pombo A, Crippa MP. Poised transcription factories prime silent uPA gene prior to activation. PLoS Biol. 2010;8(1):e1000270.**

21. **Dixon JR, Selvaraj S, Yue F, Kim A, Li Y, Shen Y, Hu M, Liu JS, Ren B. Topological domains in mammalian genomes identified by analysis of chromatin interactions. Nature. 2012;485(7398):376-80.**

22. **Rajapakse I, Scalzo D, Tapscott SJ, Kosak ST, Groudine M. Networking the nucleus. Mol Syst Biol. 2010;6:395.**

23. **Misteli T. Self-organization in the genome. Proc Natl Acad Sci U S A. 2009;106(17):6885-6.**

24. **Soutoglou E, Misteli T. Activation of the cellular DNA damage response in the absence of DNA lesions. Science. 2008;320(5882):1507-10.**

25. **Kaiser TE, Intine RV, Dundr M. De novo formation of a subnuclear body. Science. 2008;322(5908):1713-7.**

26. **Wood AM, Garza-Gongora AG, Kosak ST. A Crowdsourced nucleus: understanding nuclear organization in terms of dynamically networked protein function. Biochim Biophys Acta. 2014;1839(3):178-90.**

27. **Mitchell JA, Fraser P. Transcription factories are nuclear subcompartments that remain in the absence of transcription. Genes Dev. 2008;22(1):20-5.**

28. **Shaklai S, Amariglio N, Rechavi G, Simon AJ. Gene silencing at the nuclear periphery. FEBS J. 2007;274(6):1383-92.**

29. **Reddy KL, Zullo JM, Bertolino E, Singh H. Transcriptional repression mediated by repositioning of genes to the nuclear lamina. Nature. 2008;452(7184):243-7.**

30. Dundr M. Nuclear bodies: multifunctional companions of the genome. Curr Opin Cell Biol. 2012;24(3):415-22.

31. Gorisch SM, Wachsmuth M, Ittrich C, Bacher CP, Rippe K, Lichter P. Nuclear body movement is determined by chromatin accessibility and dynamics. Proc Natl Acad Sci U S A. 2004;101(36):13221-6.

32. Carmo-Fonseca M, Berciano MT, Lafarga M. Orphan nuclear bodies. Cold Spring Harb Perspect Biol. 2010;2(9):a000703.

33. Bernardi R, Pandolfi PP. Structure, dynamics and functions of promyelocytic leukaemia nuclear bodies. Nat Rev Mol Cell Biol. 2007;8(12):1006-16.

34. Lallemand-Breitenbach V, de The H. PML nuclear bodies. Cold Spring Harb Perspect Biol. 2010;2(5):a000661.

35. Ascoli CA, Maul GG. Identification of a novel nuclear domain. J Cell Biol. 1991;112(5):785-95.

36. Batty E, Jensen K, Freemont P. PML nuclear bodies and their spatial relationships in the mammalian cell nucleus. Front Biosci (Landmark Ed). 2009;14:1182-96.

37. Chang CC, Naik MT, Huang YS, Jeng JC, Liao PH, Kuo HY, Ho CC, Hsieh YL, Lin CH, Huang NJ, Naik NM, Kung CC, Lin SY, Chen RH, Chang KS, Huang TH, Shih HM. Structural and functional roles of Daxx SIM phosphorylation in SUMO paralog-selective binding and apoptosis modulation. Mol Cell. 2011;42(1):62-74.

38. Zhong S, Salomoni P, Ronchetti S, Guo A, Ruggero D, Pandolfi PP. Promyelocytic leukemia protein (PML) and Daxx participate in a novel nuclear pathway for apoptosis. J Exp Med. 2000;191(4):631-40.

39. David A, Dolan BP, Hickman HD, Knowlton JJ, Clavarino G, Pierre P, Bennink JR, Yewdell JW. Nuclear translation visualized by ribosome-bound nascent chain puromycylation. J Cell Biol. 2012;197(1):45-57.

40. Iborra FJ, Jackson DA, Cook PR. Coupled transcription and translation within nuclei of mammalian cells. Science. 2001;293(5532):1139-42.

41. Lykke-Andersen J, Bennett EJ. Protecting the proteome: Eukaryotic cotranslational quality control pathways. J Cell Biol. 2014;204(4):467-76.

42. Shiels C, Islam SA, Vatcheva R, Sasieni P, Sternberg MJ, Freemont PS, Sheer D. PML bodies associate specifically with the MHC gene cluster in interphase nuclei. J Cell Sci. 2001;114(Pt 20):3705-16.

43. Ching RW, Ahmed K, Boutros PC, Penn LZ, Bazett-Jones DP. Identifying gene locus associations with promyelocytic leukemia nuclear bodies using immuno-TRAP. J Cell Biol. 2013;201(2):325-35.

44. Wang Q, Sawyer IA, Sung MH, Sturgill D, Shevtsov SP, Pegoraro G, Hakim O, Baek S, Hager GL, Dundr M. Cajal bodies are linked to genome conformation. Nat Commun. 2016;7:10966.

45. Shimi T, Butin-Israeli V, Goldman RD. The functions of the nuclear envelope in mediating the molecular crosstalk between the nucleus and the cytoplasm. Curr Opin Cell Biol. 2012;24(1):71-8.

46. Khatau SB, Hale CM, Stewart-Hutchinson PJ, Patel MS, Stewart CL, Searson PC, Hodzic D, Wirtz D. A perinuclear actin cap regulates nuclear shape. Proc Natl Acad Sci U S A. 2009;106(45):19017-22.

47. Versaevel M, Grevesse T, Gabriele S. Spatial coordination between cell and nuclear shape within micropatterned endothelial cells. Nat Commun. 2012;3:671.

48. Iyer KV, Pulford S, Mogilner A, Shivashankar GV. Mechanical activation of cells induces chromatin remodeling preceding MKL nuclear transport. Biophys J. 2012;103(7):1416-28.

49. Poh YC, Shevtsov SP, Chowdhury F, Wu DC, Na S, Dundr M, Wang N. Dynamic force-induced direct dissociation of protein complexes in a nuclear body in living cells. Nat Commun. 2012;3:866.

50. Dupont S, Morsut L, Aragona M, Enzo E, Giulitti S, Cordenonsi M, Zanconato F, Le Digabel J, Forcato M, Bicciato S, Elvassore N, Piccolo S. Role of YAP/TAZ in mechanotransduction. Nature. 2011;474(7350):179-83.

51. Etienne-Manneville S. Cdc42--the centre of polarity. J Cell Sci. 2004;117(Pt 8):1291-300.

52. Fuchs E, Raghavan S. Getting under the skin of epidermal morphogenesis. Nat Rev Genet. 2002;3(3):199-209.

53. Fuchs E. Epidermal differentiation: the bare essentials. J Cell Biol. 1990;111(6 Pt 2):2807-14.

54. Ridley AJ, Schwartz MA, Burridge K, Firtel RA, Ginsberg MH, Borisy G, Parsons JT, Horwitz AR. Cell migration: integrating signals from front to back. Science. 2003;302(5651):1704-9.

55. Mayor R, Etienne-Manneville S. The front and rear of collective cell migration. Nat Rev Mol Cell Biol. 2016;17(2):97-109.

56. Nelson WJ. Remodeling epithelial cell organization: transitions between front-rear and apical-basal polarity. Cold Spring Harb Perspect Biol. 2009;1(1):a000513.

57. Peinado H, Olmeda D, Cano A. Snail, Zeb and bHLH factors in tumour progression: an alliance against the epithelial phenotype? Nat Rev Cancer. 2007;7(6):415-28.

58. Hopkinson SB, Hamill KJ, Wu Y, Eisenberg JL, Hiroyasu S, Jones JC. Focal Contact and Hemidesmosomal Proteins in Keratinocyte Migration and Wound Repair. Adv Wound Care (New Rochelle). 2014;3(3):247-263.

59. Mehta K, Gunasekharan V, Satsuka A, Laimins LA. Human papillomaviruses activate and recruit SMC1 cohesin proteins for the differentiation-dependent life cycle through association with CTCF insulators. PLoS Pathog. 2015;11(4):e1004763.

60. McCance DJ, Kopan R, Fuchs E, Laimins LA. Human papillomavirus type 16 alters human epithelial cell differentiation in vitro. Proc Natl Acad Sci U S A. 1988;85(19):7169-73.

61. Asselineau D, Prunieras M. Reconstruction of 'simplified' skin: control of fabrication. Br J Dermatol. 1984;111 Suppl 27:219-22.

62. Zufferey R, Dull T, Mandel RJ, Bukovsky A, Quiroz D, Naldini L, Trono D. Self-inactivating lentivirus vector for safe and efficient in vivo gene delivery. J Virol. 1998;72(12):9873-80.

63. Mueller F, Senecal A, Tantale K, Marie-Nelly H, Ly N, Collin O, Basyuk E, Bertrand E, Darzacq X, Zimmer C. FISH-quant: automatic counting of transcripts in 3D FISH images. Nat Methods. 2013;10(4):277-8.

64. Simpson CL, Patel DM, Green KJ. Deconstructing the skin: cytoarchitectural determinants of epidermal morphogenesis. Nat Rev Mol Cell Biol. 2011;12(9):565-80.

65. Meyers C, Laimins LA. In vitro systems for the study and propagation of human papillomaviruses. Curr Top Microbiol Immunol. 1994;186:199-215.

66. Fedorova E, Zink D. Nuclear architecture and gene regulation. Biochim Biophys Acta. 2008;1783(11):2174-84.

67. Madrazo E, Conde AC, Redondo-Munoz J. Inside the Cell: Integrins as New Governors of Nuclear Alterations? Cancers (Basel). 2017;9(7).

68. Poumay Y, Roland IH, Leclercq-Smekens M, Leloup R. Basal detachment of the epidermis using dispase: tissue spatial organization and fate of integrin alpha 6 beta 4 and hemidesmosomes. J Invest Dermatol. 1994;102(1):111-7.

69. Wilhelmsen K, Litjens SH, Kuikman I, Tshimbalanga N, Janssen H, van den Bout I, Raymond K, Sonnenberg A. Nesprin-3, a novel outer nuclear membrane protein, associates with the cytoskeletal linker protein plectin. J Cell Biol. 2005;171(5):799-810.

70. Stewart-Hutchinson PJ, Hale CM, Wirtz D, Hodzic D. Structural requirements for the assembly of LINC complexes and their function in cellular mechanical stiffness. Exp Cell Res. 2008;314(8):1892-905.

71. Chang W, Worman HJ, Gundersen GG. Accessorizing and anchoring the LINC complex for multifunctionality. J Cell Biol. 2015;208(1):11-22.

72. Isermann P, Lammerding J. Nuclear mechanics and mechanotransduction in health and disease. Curr Biol. 2013;23(24):R1113-21.

73. Lombardi ML, Jaalouk DE, Shanahan CM, Burke B, Roux KJ, Lammerding J. The interaction between nesprins and sun proteins at the nuclear envelope is critical for force transmission between the nucleus and cytoskeleton. J Biol Chem. 2011;286(30):26743-53.

74. Schneider M, Lu W, Neumann S, Brachner A, Gotzmann J, Noegel AA, Karakesisoglou I. Molecular mechanisms of centrosome and cytoskeleton anchorage at the nuclear envelope. Cell Mol Life Sci. 2011;68(9):1593-610.

75. Lu W, Schneider M, Neumann S, Jaeger VM, Taranum S, Munck M, Cartwright S, Richardson C, Carthew J, Noh K, Goldberg M, Noegel AA, Karakesisoglou I. Nesprin interchain associations control nuclear size. Cell Mol Life Sci. 2012;69(20):3493-509.

76. Hebert AM, DuBoff B, Casaletto JB, Gladden AB, McClatchey AI. Merlin/ERM proteins establish cortical asymmetry and centrosome position. Genes Dev. 2012;26(24):2709-23.

77. Raj A, van den Bogaard P, Rifkin SA, van Oudenaarden A, Tyagi S. Imaging individual mRNA molecules using multiple singly labeled probes. Nat Methods. 2008;5(10):877-9.

78. Strickfaden H, Zunhammer A, van Koningsbruggen S, Kohler D, Cremer T. 4D chromatin dynamics in cycling cells: Theodor Boveri's hypotheses revisited. Nucleus. 2010;1(3):284-97.

79. Chubb JR, Boyle S, Perry P, Bickmore WA. Chromatin motion is constrained by association with nuclear compartments in human cells. Curr Biol. 2002;12(6):439-45.

80. Thomson I, Gilchrist S, Bickmore WA, Chubb JR. The radial positioning of chromatin is not inherited through mitosis but is established de novo in early G1. Curr Biol. 2004;14(2):166-72.

81. Golloshi R, Sanders JT, McCord RP. Genome organization during the cell cycle: unity in division. Wiley Interdiscip Rev Syst Biol Med. 2017;9(5).

82. Khanna N, Hu Y, Belmont AS. HSP70 transgene directed motion to nuclear speckles facilitates heat shock activation. Curr Biol. 2014;24(10):1138-44.

83. Mehta IS, Amira M, Harvey AJ, Bridger JM. Rapid chromosome territory relocation by nuclear motor activity in response to serum removal in primary human fibroblasts. Genome Biol. 2010;11(1):R5.

84. Mehta IS, Kulashreshtha M, Chakraborty S, Kolthur-Seetharam U, Rao BJ. Chromosome territories reposition during DNA damage-repair response. Genome Biol. 2013;14(12):R135.

85. Kulashreshtha M, Mehta IS, Kumar P, Rao BJ. Chromosome territory relocation during DNA repair requires nuclear myosin 1 recruitment to chromatin mediated by Upsilon-H2AX signaling. Nucleic Acids Res. 2016;44(17):8272-91.

86. Chuang CH, Carpenter AE, Fuchsova B, Johnson T, de Lanerolle P, Belmont AS. Long-range directional movement of an interphase chromosome site. Curr Biol. 2006;16(8):825-31.

87. Dundr M, Ospina JK, Sung MH, John S, Upender M, Ried T, Hager GL, Matera AG. Actin-dependent intranuclear repositioning of an active gene locus in vivo. J Cell Biol. 2007;179(6):1095-103.

88. Kind J, Pagie L, Ortabozkoyun H, Boyle S, de Vries SS, Janssen H, Amendola M, Nolen LD, Bickmore WA, van Steensel B. Single-cell dynamics of genome-nuclear lamina interactions. Cell. 2013;153(1):178-92.

89. Rajapakse I, Perlman MD, Scalzo D, Kooperberg C, Groudine M, Kosak ST. The emergence of lineage-specific chromosomal topologies from coordinate gene regulation. Proc Natl Acad Sci U S A. 2009;106(16):6679-84.

90. Park S, Gonzalez DG, Guirao B, Boucher JD, Cockburn K, Marsh ED, Mesa KR, Brown S, Rompolas P, Haberman AM, Bellaiche Y, Greco V. Tissue-scale coordination of cellular behaviour promotes epidermal wound repair in live mice. Nat Cell Biol. 2017;19(2):155-163.

91. Houben F, Willems CH, Declercq IL, Hochstenbach K, Kamps MA, Snoeckx LH, Ramaekers FC, Broers JL. Disturbed nuclear orientation and cellular migration in A-type lamin deficient cells. Biochim Biophys Acta. 2009;1793(2):312-24.

92. Levy JR, Holzbaur EL. Dynein drives nuclear rotation during forward progression of motile fibroblasts. J Cell Sci. 2008;121(Pt 19):3187-95.

93. Maninova M, Klimova Z, Parsons JT, Weber MJ, Iwanicki MP, Vomastek T. The reorientation of cell nucleus promotes the establishment of front-rear polarity in migrating fibroblasts. J Mol Biol. 2013;425(11):2039-55.

94. Burute M, Prioux M, Blin G, Truchet S, Letort G, Tseng Q, Bessy T, Lowell S, Young J, Filhol O, Thery M. Polarity Reversal by Centrosome Repositioning Primes Cell Scattering during Epithelial-to-Mesenchymal Transition. Dev Cell. 2017;40(2):168-184.

95. Luxton GW, Gomes ER, Folker ES, Vintinner E, Gundersen GG. Linear arrays of nuclear envelope proteins harness retrograde actin flow for nuclear movement. Science. 2010;329(5994):956-9.

96. Ji JY, Lee RT, Vergnes L, Fong LG, Stewart CL, Reue K, Young SG, Zhang Q, Shanahan CM, Lammerding J. Cell nuclei spin in the absence of lamin b1. J Biol Chem. 2007;282(27):20015-26.

97. Neems DS, Garza-Gongora AG, Smith ED, Kosak ST. Topologically associated domains enriched for lineage-specific genes reveal expression-dependent nuclear topologies during myogenesis. Proc Natl Acad Sci U S A. 2016;113(12):E1691-700.

98. Ferrai C, de Castro IJ, Lavitas L, Chotalia M, Pombo A. Gene positioning. Cold Spring Harb Perspect Biol. 2010;2(6):a000588.

99. Bank EM, Gruenbaum Y. The nuclear lamina and heterochromatin: a complex relationship. Biochem Soc Trans. 2011;39(6):1705-9.

100. Shestakova EA, Singer RH, Condeelis J. The physiological significance of beta - actin mRNA localization in determining cell polarity and directional motility. Proc Natl Acad Sci U S A. 2001;98(13):7045-50.

101. Eliscovich C, Singer RH. RNP transport in cell biology: the long and winding road. Curr Opin Cell Biol. 2017;45:38-46.

102. Shav-Tal Y, Darzacq X, Shenoy SM, Fusco D, Janicki SM, Spector DL, Singer RH. Dynamics of single mRNPs in nuclei of living cells. Science. 2004;304(5678):1797-800.

103. Mor A, Suliman S, Ben-Yishay R, Yunger S, Brody Y, Shav-Tal Y. Dynamics of single mRNP nucleocytoplasmic transport and export through the nuclear pore in living cells. Nat Cell Biol. 2010;12(6):543-52.

104. Park HY, Lim H, Yoon YJ, Follenzi A, Nwokafor C, Lopez-Jones M, Meng X, Singer RH. Visualization of dynamics of single endogenous mRNA labeled in live mouse. Science. 2014;343(6169):422-4.

105. Chen H, Larson DR. What have single-molecule studies taught us about gene expression? Genes Dev. 2016;30(16):1796-810.

106. Florian MC, Dorr K, Niebel A, Daria D, Schrezenmeier H, Rojewski M, Filippi MD, Hasenberg A, Gunzer M, Scharffetter-Kochanek K, Zheng Y, Geiger H. Cdc42 activity regulates hematopoietic stem cell aging and rejuvenation. Cell Stem Cell. 2012;10(5):520-30.

107. Campanale JP, Sun TY, Montell DJ. Development and dynamics of cell polarity at a glance. J Cell Sci. 2017;130(7):1201-1207.

108. Kosak ST, Groudine M. Form follows function: The genomic organization of cellular differentiation. Genes Dev. 2004;18(12):1371-84.

109. Joffe B, Leonhardt H, Solovei I. Differentiation and large scale spatial organization of the genome. Curr Opin Genet Dev. 2010;20(5):562-9.

110. Gdula MR, Poterlowicz K, Mardaryev AN, Sharov AA, Peng Y, Fessing MY, Botchkarev VA. Remodeling of three-dimensional organization of the nucleus during terminal keratinocyte differentiation in the epidermis. J Invest Dermatol. 2013;133(9):2191-201.

111. Kosak ST, Skok JA, Medina KL, Riblet R, Le Beau MM, Fisher AG, Singh H. Subnuclear compartmentalization of immunoglobulin loci during lymphocyte development. Science. 2002;296(5565):158-62.